nature immunology

ARTICLES

https://doi.org/10.1038/s41590-021-00968-4

Check for updates

Distinct transcription factor networks control neutrophil-driven inflammation

Tariq E. Khoyratty[1,4], Zhichao Ai[1,4], Ivan Ballesteros[2], Hayley L. Eames[1], Sara Mathie[1], Sandra Martín-Salamanca[2], Lihui Wang[1], Ashleigh Hemmings[1], Nicola Willemsen[1], Valentin von Werz[1], Annette Zehrer[3], Barbara Walzog[3], Erinke van Grinsven[1], Andres Hidalgo[2] and Irina A. Udalova[1]✉

Neutrophils display distinct gene expression patters depending on their developmental stage, activation state and tissue microenvironment. To determine the transcription factor networks that shape these responses in a mouse model, we integrated transcriptional and chromatin analyses of neutrophils during acute inflammation. We showed active chromatin remodeling at two transition stages: bone marrow–to-blood and blood-to-tissue. Analysis of differentially accessible regions revealed distinct sets of putative transcription factors associated with control of neutrophil inflammatory responses. Using ex vivo and in vivo approaches, we confirmed that RUNX1 and KLF6 modulate neutrophil maturation, whereas RELB, IRF5 and JUNB drive neutrophil effector responses and RFX2 and RELB promote survival. Interfering with neutrophil activation by targeting one of these factors, JUNB, reduced pathological inflammation in a mouse model of myocardial infarction. Therefore, our study represents a blueprint for transcriptional control of neutrophil responses in acute inflammation and opens possibilities for stage-specific therapeutic modulation of neutrophil function in disease.

Neutrophils are important effector cells of the innate immune system and are produced in large numbers in the bone marrow through stepwise differentiation of myeloid progenitors, featuring distinct morphological changes and stage-specific expression pattern of surface receptors[1–3]. On entering the circulation, they patrol blood vessels and tissues for microbial and sterile challenges. Neutrophil functional responses are diverse, including but not limited to phagocytosis, generation of reactive oxygen species (ROS) and production of cytokines and other inflammatory factors, to influence and regulate inflammatory as well as adaptive immune responses[4,5]. However, neutrophil populations are not homogeneous[4,6–8]. Increasing evidence supports the notion that neutrophils are transcriptionally active cells[9–12]. They possess the ability to adapt their genome accessibility and change the transcriptional program en route to naive tissues[13] and exhibit phenotypic and functional heterogeneity in various immune disorders and cancers[7,14–16]. However, the cell-intrinsic molecular regulators orchestrating adaptations in neutrophil phenotype and function remain largely unexplored.

There is partial understanding of the transcription factors that promote neutrophil differentiation. PU.1 and CCAAT/enhancer-binding protein α (C/EBPα), are essential for neutrophilic lineage commitment and early differentiation[17,18]; C/EBPε and growth factor independent protein 1 (Gfi-1) function in promoting neutrophil terminal differentiation[2,19] and C/EBPβ regulates emergency granulopoiesis[20]. These and other transcription factors instruct a transcriptional program that allows developmental transition from neutrophil precursors into mature neutrophils[21,22].

Mature neutrophils possess the full range of effector functions, including ROS production, phagocytosis and chemotaxis, which enable rapid responses to stimulation and orchestration of protective immunity[2,11]. Under different activating conditions, they additionally upregulate the expression of genes involved in cytokine production and pathogen clearance[11,23]. Multiple signaling pathways activated during neutrophil stimulation are predicted to converge at common transcription factors, which are utilized in a combinatorial manner depending on the activating stimuli. These include interferon regulatory factors, CCAAT-enhancer-binding proteins and NF-κB family members, which together orchestrate inflammatory responses[9,24].

Recent single-cell RNA sequencing (scRNA-seq) of murine neutrophils revealed a heterogeneous and complex neutrophil population under steady-state and bacterial infection conditions and proposed neutrophil-specific networks, including previously reported transcription factors and new regulons[11]. However, which of the proposed multitude of regulators actually control neutrophil differentiation and activation is unknown. In this study, we combined transcriptional and chromatin profiling of neutrophils en route to sites of inflammation with genetic perturbation approaches to identify and functionally validate key regulators of neutrophil function in inflammation.

Results

Inflammatory neutrophils are under dynamic transcriptional control. To identify putative transcription factors in control of neutrophil inflammatory responses, we assessed chromatin and transcriptional changes during neutrophil recruitment and activation in the air pouch model of acute inflammation (Fig. 1a), which provides a robust and reliable method to quantify early neutrophil infiltration into the tissue lining and air pouch cavity[25].

[1]Kennedy Institute of Rheumatology, University of Oxford, Oxford, UK. [2]Area of Cell & Developmental Biology, Centro Nacional de Investigaciones Cardiovasculares Carlos III, Madrid, Spain. [3]Institute of Cardiovascular Physiology and Pathophysiology, Biomedical Center and Walter Brendel Center of Experimental Medicine, University Hospital, Ludwig-Maximilians-University Munich, Munich, Germany. [4]These authors contributed equally: Tariq E. Khoyratty, Zhichao Ai. ✉e-mail: Irina.udalova@kennedy.ox.ac.uk

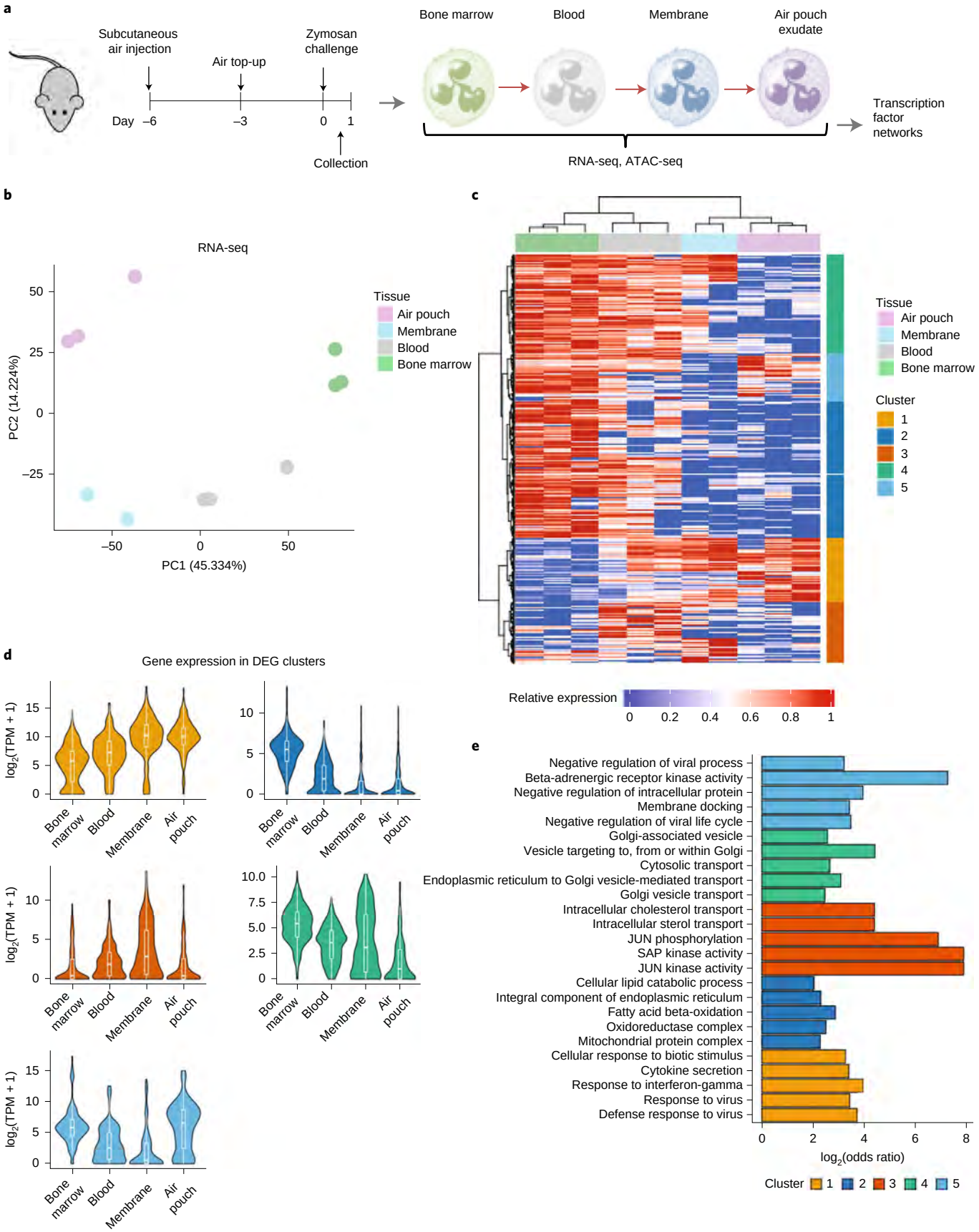

In this model, a cavity is created on the dorsal surface of mice and granulation tissue (membrane) is formed over a period of 6 d (Extended Data Fig. 1a), composed primarily of fibroblasts and macrophages[26–28]. Injection of 1 mg of zymosan, a ligand for dectin-1 and Toll-like receptor 2/6, into the pouch cavity results in efficient infiltration of immune cells from the blood into the

Fig. 1 | Neutrophil transcriptional rewiring en route to the site of inflammation is parsimonious. a, Ly6G^{hi} CD11b^{+} cells were sorted from the bone marrow, blood, air pouch membrane and air pouch exudate in mice subjected to the air pouch model and zymosan challenge for 4 h. Small bulk RNA-seq analysis powered by Smart-seq2 library preparations[52] for transcriptional changes and ATAC-seq analysis for chromatin changes were conducted. **b**, PCA of 1,865 DEGs derived from small bulk RNA-seq analysis ($n = 300$ cells per sample) of neutrophils isolated from the bone marrow, blood, membrane and exudate of two mice subjected to the air pouch model and zymosan challenge. **c**, Hierarchical clustering of all DEGs (likelihood ratio test, $P_{adj} < 0.01$), based on Manhattan distances using the Ward method. Data are presented as a heatmap normalized to the minimum and maximum of each row. **d**, Violin plots showing the expression of all genes within each cluster identified in **b** across different compartments from two mice. For the box plot within each violin plot, the middle lines indicate the median values, the boxes range from the 25th to 75th percentiles and the upper and lower whiskers extend from the hinge to the largest and smallest value, respectively, no further than 1.5 times the interquartile range from the hinge. **e**, GO analysis, showing the top five enriched GO categories for each cluster from Fig. 1c.

membrane and pouch (Supplementary Data), a large proportion being neutrophils[29]. Neutrophil recruitment initiated at 4 h (Supplementary Data), and peaked at 12 h after stimulation in the pouch (Extended Data Fig. 1c), while remaining up to 24 h in the membrane (Extended Data Fig. 1d). Phenotypic assessment of neutrophils from the blood, membrane and pouch at 4 h post-zymosan challenge revealed progressively elevated levels of intracellular pro-interleukin 1-β (IL-1β) in the membrane and pouch, indicating that neutrophils undergo activation as they traverse to the tissue (Extended Data Fig. 1e).

We isolated Ly6G^{hi} CD11b^{+} cells from the bone marrow, blood, membrane and air pouch exudate 4 h after challenge with zymosan (Extended Data Fig. 1f) and conducted small bulk messenger RNA-seq and assay for transposase-accessible chromatin using sequencing (ATAC-seq) analyses (Fig. 1a). In zymosan-challenged animals, a substantial proportion of neutrophils in the blood, air pouch membrane and exudate expressed CD101 (Extended Data Fig. 1g), a marker of mature neutrophils[2], whereas bone marrow neutrophils were largely CD101^{-} and represented immature neutrophils (Extended Data Fig. 1g,h). Zymosan challenge induced egress of bone marrow immature neutrophils into the circulation, which were largely absent in naive mice (Extended Data Fig. 1h).

First, we mapped the transcriptional changes associated with neutrophil progression to the site of inflammation in vivo (Fig. 1a). Principal component analysis (PCA) of 1,865 differentially expressed genes (DEGs) ($P_{adj} < 0.1$) clearly separated neutrophils from the compartments and indicated that changes were incremental, initiating with the transition from the bone marrow to the blood and continuing gradually as neutrophils migrate into sites of inflammation (Fig. 1b). Comparison between the bone marrow and air pouch neutrophils revealed 445 upregulated and 1,303 downregulated genes (Extended Data Fig. 2a). Gene set enrichment analysis (GSEA) of DEGs between the air pouch and bone marrow ($P_{adj} < 0.05$ and fold change >1.5) revealed that chemotaxis, cytokine activity and signaling pathway genes are gradually upregulated along the maturation trajectory and the inflammatory cascade, while respiratory chain complex, mitochondrial matrix and fatty acid beta-oxidation genes are gradually downregulated (Fig. 1c and Extended Data Fig. 2b,c).

Hierarchical clustering of the DEGs across all the compartments identified five clusters (Fig. 1c), which encompass genes progressively upregulated in the blood, membrane and air pouch (cluster 1), transiently upregulated in the blood (cluster 3), rapidly downregulated in the membrane and air pouch (cluster 2), slowly downregulated in the air pouch (cluster 4) and transiently downregulated in the blood (cluster 5) (Fig. 1d). Gene ontology (GO) analysis revealed that downregulated genes in clusters 2 and 4 primarily correlated to metabolic processes (cluster 2: cellular lipid catabolism, fatty acid beta oxidation) and protein transport (cluster 4: cytosolic transport, Golgi vesicle transport) (Fig. 1e). The upregulated genes in cluster 3 represent stress response JNK/SAP kinases; in cluster 1, they are pro-inflammatory and interferon response genes (cytokine secretion, response to interferon gamma) (Fig. 1e).

Overall, our global analyses of the transcriptional landscape during inflammation reveals loss of anabolic capacity as neutrophils leave the bone marrow, transient reduction in their toxic potential coupled with gain of signal transduction in the circulation and final acquisition of an inflammatory and effector profile at the site of challenge.

Chromatin changes underpin transcriptional activation. Second, we mapped chromatin changes associated with neutrophil activation in vivo (Fig. 1a). The PCA analysis of 11,881 differentially accessible peaks (DAPs) derived from ATAC-seq analysis ($P_{adj} < 0.05$) revealed marked diversity in chromatin landscapes between neutrophils in the bone marrow, blood and membrane (Fig. 2a); therefore, chromatin remodeling is likely to underpin the changes in transcriptional profiles seen along the inflammatory cascade. Remarkably, we observed no further chromatin remodeling events at the transition from inflamed tissue to exudate (Fig. 2a), suggesting that the detected change in gene expression at this final step of neutrophil migration does not require global alterations in transcriptional control.

The ATAC-seq analyses identified two distinct remodeling events, the transition of neutrophils from bone marrow to blood (481 opening and 356 closing peaks) and from blood to the inflamed tissue (2,150 opening and 878 closing peaks) (Extended Data Fig. 3a). For instance, accessibility of the myeloid differentiation marker *Myadm* increased as neutrophils were released into the blood,

Fig. 2 | Neutrophils dynamically alter their chromatin landscape en route to the site of inflammation. a, ATAC-seq analysis was conducted on Ly6G^{hi} CD11b^{+} cells sorted from the bone marrow, blood, membrane and air pouch exudate in mice subjected to the air pouch model and zymosan challenge for 4 h. ATAC-seq peak calling with MACS2 revealed 47,164 peaks detected across all 4 neutrophil stages. PCA of 11,881 DAPs derived from ATAC-seq analysis ($n = 50{,}000$ cells per sample) of neutrophils isolated from the bone marrow, blood, membrane and exudate of two mice subjected to the air pouch model and zymosan challenge. **b**, Representative snapshots of normalized read counts (fragments per kilobase of transcript per million mapped reads (FPMK)) at gene loci. **c**, Distribution histogram of DAPs over 5-kb regions centered on the peaks (2.5 kb either side of the peak) in neutrophils from different compartments. **d**, Intersection of RNA-seq and ATAC-seq data: genes that are both upregulated and located in the regions of opening ATAC-seq peaks (increased chromatin accessibility) (as in Fig. 2b) are highlighted in red; genes that are both downregulated and located in the regions of closing ATAC-seq peaks (decreased chromatin accessibility) are highlighted in blue. **e**, GO analysis of genes that are differentially expressed and located in differentially accessible regions (as in Fig. 2c). The top six GO terms for upregulated genes with opening peaks (red) and downregulated genes with closing peaks (blue) are shown. **f**, De novo motif enrichment analysis for ATAC-seq peaks increasing (left) and decreasing (right) in accessibility using MEME-ChIP. Numbers indicate adjusted *P* values.

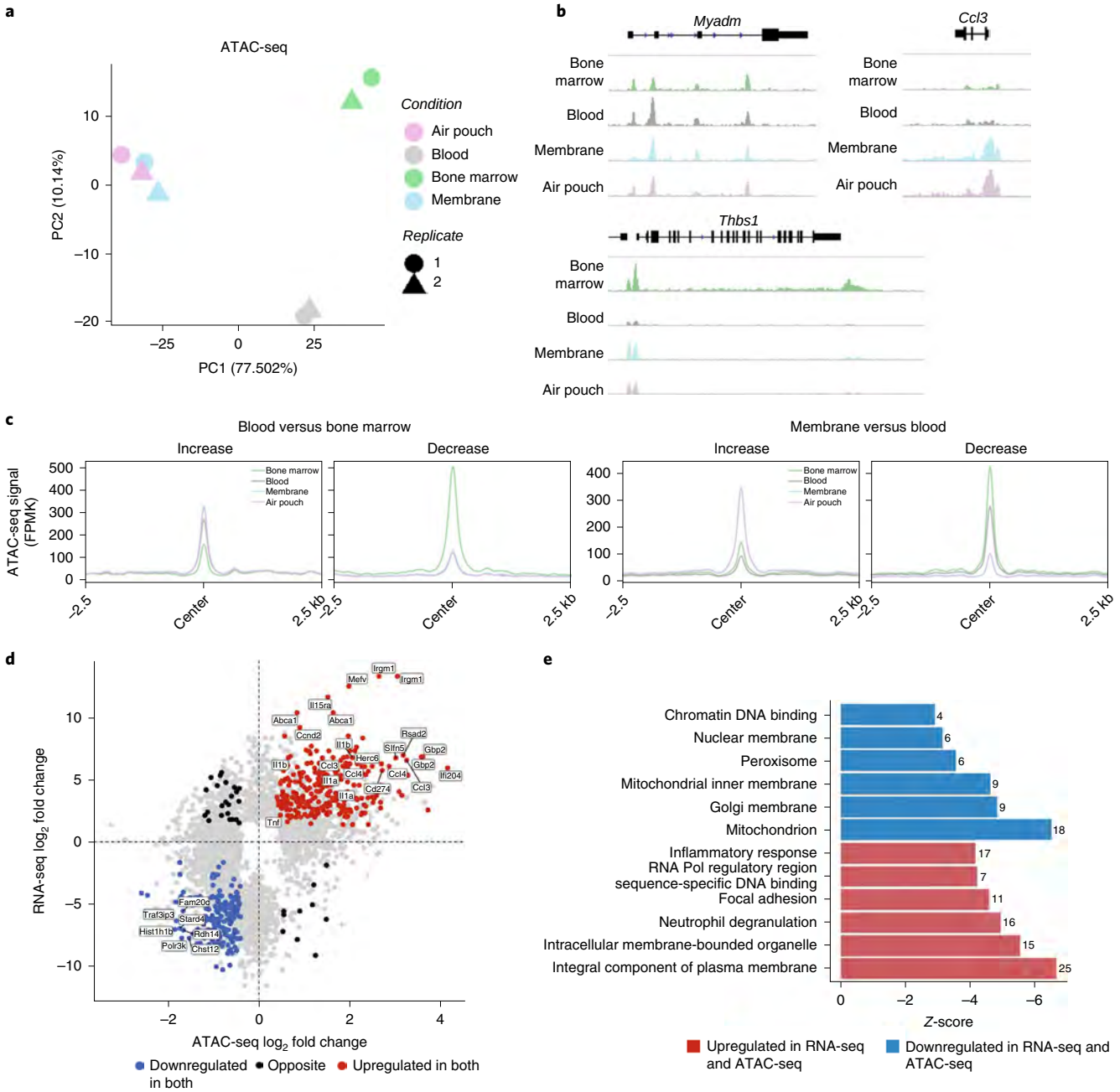

f

Opening peaks

Motif	Transcription factor family	P_{adj}	Comparison
	PU.1	1.4×10^{-138}	Blood versus bone marrow
	AP-1	3.4×10^{-87}	Blood versus bone marrow
	RFX	1.8×10^{-11}	Blood versus bone marrow
	AP-1	1.6×10^{-283}	Membrane versus blood
	PU.1	2.3×10^{-69}	Membrane versus blood
	NF-κB	9.5×10^{-23}	Membrane versus blood
	IRF	3.5×10^{-9}	Membrane versus blood

Closing peaks

Motif	Transcription factor family	P_{adj}	Comparison
	PU.1	2.3×10^{-28}	Blood versus bone marrow
	SP/KLF	2.2×10^{-12}	Blood versus bone marrow
	PU.1	7.1×10^{-418}	Membrane versus blood
	SP/KLF	1.4×10^{-41}	Membrane versus blood
	SP/KLF	1.5×10^{-14}	Membrane versus blood
	RUNX	1.1×10^{-3}	Membrane versus blood

whereas the *Thbs1* locus closed. In turn, the basally inaccessible promoter of *Ccl3* opened drastically once neutrophils reached the site of inflammation (Fig. 2b). The analysis of DAPs over 5 kilobase (kb) regions centered on the peaks revealed comparable number of peaks with increased and decreased accessibility at the two transition points: bone marrow to blood and blood to tissue (Fig. 2c and Extended Data Fig. 3b). It suggested that neutrophil reprogramming is parsimonious and under strict control.

Fig. 3 | RUNX1 and KLF6 deficiency impairs the maturation of neutrophils. a, Morphology assessment of WT and indicated knockout HoxB8 neutrophils differentiated for 5 days. Scale bar, 10 μm. Representative images from three independent experiments are shown. **b**, Quantification of different maturation stages in WT and transcription factor–deficient HoxB8 neutrophils as in **a**. The results are expressed as percentages of segmented band neutrophils and metamyelocyte and at least 200 cells counted from different fields. Data are shown as the mean and s.d. from three independent experiments. Significant differences compared with the WT control group are denoted as: NS, not significant; $***P < 0.001$ and $****P < 0.0001$ (two-way ANOVA with Dunnett's multiple comparisons test). **c**, Differential expression of CD101 in HoxB8 neutrophils differentiated for 5 days. Data are shown as a representative of three independent experiments. **d**, Lamin-B2 (LMNB2) expression in HoxB8 neutrophils. Top: One representative western blot probed for LMNB2 and β-actin is shown. Bottom: The arbitrary units of LMNB2 expression normalized to the amount of β-actin were calculated and are shown as the mean and s.d. from three independent experiments. Significant differences compared with WT cells are denoted as $****P < 0.0001$ (ordinary one-way ANOVA with Dunnett's multiple comparisons test). **e**, OCR of WT and indicated knockout HoxB8 neutrophils. Data are shown as the mean and s.d. from three independent experiments. Significant differences compared with WT day 5 neutrophils are denoted as $*P < 0.05$, $**P < 0.01$, $***P < 0.001$ and $****P < 0.0001$ (ordinary two-way ANOVA with Tukey's multiple comparisons test). **f**, Runx1 deficiency affects neutrophil maturation in vivo. Left: Representative scatter plot of neutrophil subsets from $Runx1^{loxP/loxP}$ and $Lyz2^{Cre/Cre} \times Runx1^{loxP/loxP}$ mice. Right: Statistical analysis of percentages of indicated neutrophil subsets. **g**, *Pu.1*, *Cebpa*, *Cebpb*, *Cebpe* and *Klf6* mRNA expression in $CD11b^+$ $Ly6G^+$ neutrophils sorted from $Runx1^{loxP/loxP}$ and $Lyz2^{Cre/Cre} \times Runx1^{loxP/loxP}$ mice. **f**,**g**, Data are shown as the mean and s.d. derived from three mice. Significant differences compared with WT mice are denoted as $*P < 0.05$, $**P < 0.01$ and $****P < 0.0001$ (repeated measures two-way ANOVA with Šidák's multiple comparisons test).

Hierarchical clustering of the DAPs identified six clusters of distinct patterns of chromatin behavior, including the ones that gained or lost accessibility at the bone marrow-to-blood transition (clusters 1 and 2), at the blood-to-tissue transition (clusters 5 and 3) or transiently in blood (clusters 4 and 6) (Extended Data Fig. 3c). When DAPs were mapped to the neighboring genes, the blood-to-tissue transition was linked to increased accessibility of inflammatory response regulators and signaling pathways, while the bone marrow-to-blood transition was mainly associated with antigen presentation and metabolic activity (Extended Data Fig. 3d). Next, we compared the change in accessibility in promoter proximal peaks to that of the associated gene expression levels (Fig. 2d). The categories of genes that showed both upregulation of gene expression and increase in chromatin accessibility included the inflammatory response, neutrophil degranulation and focal adhesion (Fig. 2e).

By conducting de novo motif discovery at DAPs from bone marrow to blood and blood to tissue (membrane) we identified putative transcription factors controlling neutrophil inflammatory responses (Fig. 2f). Consistent with the known role of PU.1 in myeloid cell development[30], PU.1 motifs were detected at DAPs at both transitions (Fig. 2f). Other transcription factors displayed greater selectivity: regulatory factor X (RFX) motifs were detected exclusively at peaks with increasing accessibility from bone marrow to blood, while interferon regulatory factor (IRF) and nuclear factor kappa-light-chain-enhancer of activated B cells (NF-kB) motifs were detected at peaks with increased accessibility from blood to membrane (Fig. 2f). Activator protein 1 (AP-1) motifs were detected at both transitions but were more strongly enriched in the blood-to-membrane opening peaks. We also noted SP/KLF, and RUNX motifs at peaks with reduced accessibility from bone marrow to blood and blood to membrane. In search of transcription factors highly expressed in neutrophils, we checked the expression of each family member across immune cells (Extended Data Fig. 4a) or neutrophil populations (Extended Data Fig. 4b) at the Immunological Genome Project (ImmGen)[31]. *Rfx2* was the only gene of the RFX family and *Runx1* of the RUNX family expressed in neutrophils, while *Klf6* expression was strongest among KLF family members (Extended Data Fig. 4a). Furthermore, we queried an scRNA-seq dataset that mapped neutrophil subpopulations G0–G5 to progressively maturing neutrophils[11]. *Runx1* expression was highest at the earliest stages of neutrophil differentiation (G0–G3), whereas *RelB*, *Irf5* and *JunB* expression increased with neutrophil maturation (G4 and G5) and remained unaffected by *Escherichia coli* challenge. *Klf6* expression was detected throughout the G0–G5 populations (Extended Data Fig. 4c).

Taken together, these data suggest an incremental program of neutrophil activation, with RFX2, KLF6 and RUNX1 linked to the initial transition of neutrophils to blood and ongoing neutrophil maturation, whereas the signal-dependent transcription factors JUNB, RELB and IRF5 are predicted to play a role in the inflamed tissue.

Bone marrow-to-blood transition transcription factors control neutrophil maturation. For further functional validation of RFX2, KLF6, RUNX1, JUNB, RELB and IRF5, as well as the previously noted neutrophil transcription factors C/EBPβ[32] and CEBPε[33], we utilized a model system of immortalized myeloid HoxB8 progenitor cells, which differentiate into nonproliferating neutrophils after granulocyte colony-stimulating factor-induced ex vivo differentiation for 5 days[34]. At day 1/day 2, they resemble myelocytes/metamyelocytes and express c-Kit, CXCR4 and CD49d; at day 3/day 4 they resemble band neutrophils; at day 5, they resemble mature neutrophils expressing CXCR2 and CD101 (ref. [35]). We confirmed the highest protein levels of JUNB in day 5 neutrophils (Extended

Fig. 4 | *Runx1*$^{-/-}$ *and Klf6*$^{-/-}$ neutrophils are deficient in migration and recruitment to inflamed tissue. a, In vitro migration of HoxB8 neutrophils through a 5-μm porous membrane toward the CCL3 chemoattractant was measured by Boyden chamber migration assay. Migrated cell numbers were counted as the mean and s.d. and are representative of three independent experiments, each assessed by average cell number within different fields and independent replicates. Significant differences compared with WT cells are denoted as $*P < 0.05$, $**P < 0.01$ (repeated measures two-way ANOVA with Dunnett's multiple comparisons test). **b**, An equal mix of CellTracker Far Red–labeled WT and CellTracker CFSE–labeled knockout HoxB8 neutrophils was injected intravenously into WT mice 10 min before injection of 1 mg of zymosan into the air pouch cavity. The recruitment of neutrophils was assessed by the percentage of differentially labeled HoxB8 neutrophils recovered from the blood, air pouch membrane and air pouch exudate. **c**, Percentages of HoxB8 neutrophils recovered in the bone marrow, blood, air pouch membrane and air pouch exudate recovered from mice subjected to the air pouch model and zymosan challenge. All results are shown as the mean and s.d. from 4–6 mice within 1 experiment. Significant differences between knockout and WT neutrophils are denoted as $*P < 0.05$, $**P < 0.01$, $****P < 0.0001$ and NS (repeated measures two-way ANOVA with Šidák's multiple comparisons test). **d**, Experimental setup (left) and recruitment (right) of neutrophils. Neutrophil recruitment was assessed by the percentages of neutrophils recovered from the blood, air pouch membrane and air pouch exudate in $Runx1^{loxP/loxP}$ or $Lyz2^{Cre/Cre}Runx1^{loxP/loxP}$ mice subjected to the air pouch model and zymosan challenge. The results are shown as the mean and s.d. derived from six mice. Significant differences between $Runx1^{loxP/loxP}$ or $Lyz2^{Cre/Cre}Runx1^{loxP/loxP}$ mice are denoted as $**P < 0.01$, $****P < 0.0001$ and NS (repeated measures two-way ANOVA with Šidák's multiple comparisons test).

Data Fig. 4d), matching the mRNA expression data (Extended Data Fig. 4c) Stimulation with zymosan led to JUNB phosphorylation without affecting its protein levels (Extended Data Fig. 4d), indicating the posttranslational role of inflammatory signals in the activation of signal-dependent transcription factors.

Using CRISPR–Cas9, we generated stable knockout lines for selected transcription factors in Hoxb8 progenitors and validated their deletion by western blot analysis (Extended Data Fig. 5a). After 5 days of ex vivo differentiation, HoxB8 progenitors with genetic deletion of the *Irf5*, *JunB* or *Cepbβ* genes gave rise to

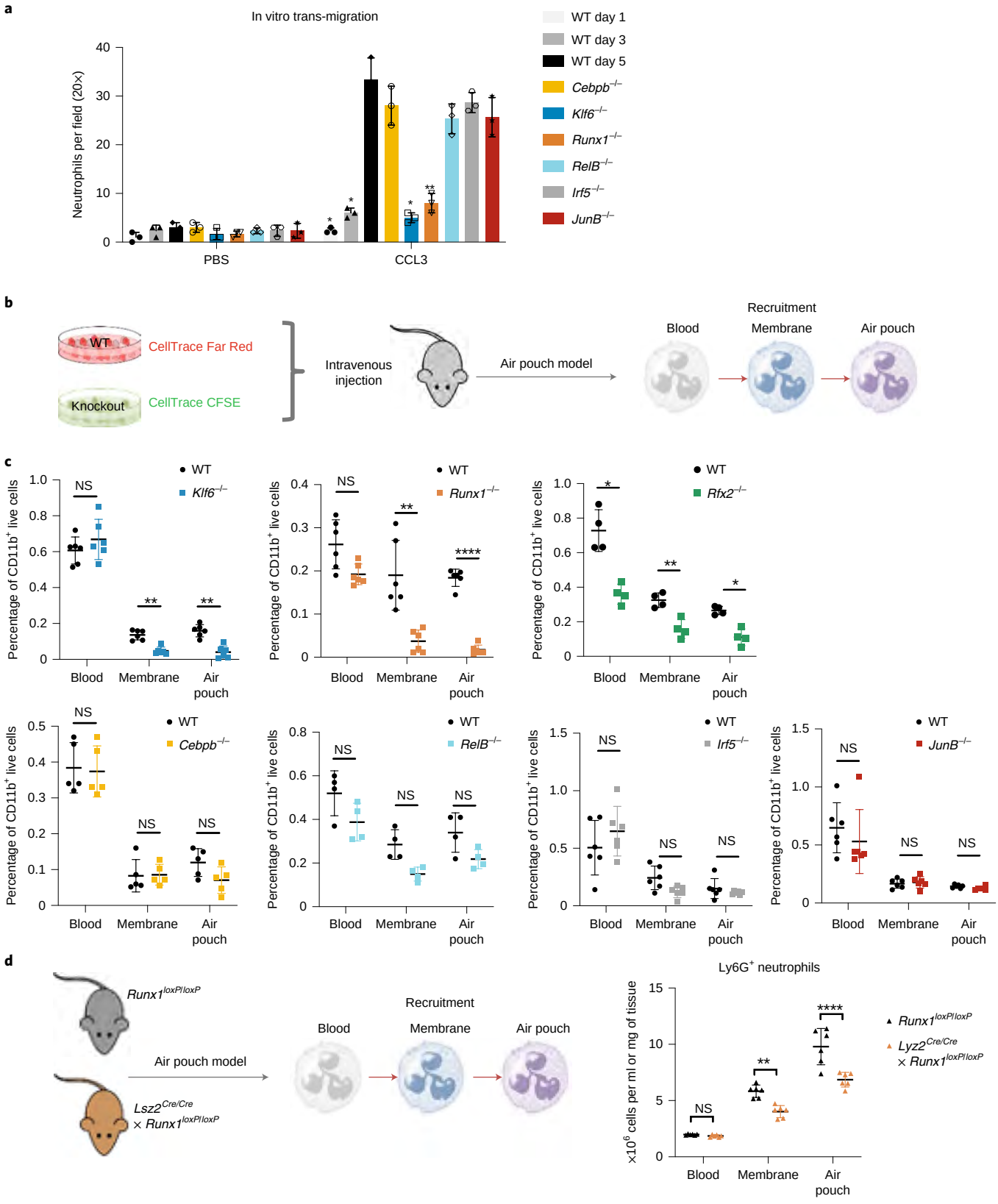

morphologically mature neutrophils, whereas *Klf6*$^{-/-}$ and *Runx1*$^{-/-}$ cells resembled a mix of band and immature neutrophils, suggesting a roadblock in neutrophil maturation (Fig. 3a,b). Deletion of *Rfx2* and *RelB* affected neutrophil maturation to a lesser extent (Fig. 3a,b). CEBPε-deficient cells did not survive beyond day 3 of ex vivo differentiation, which is consistent with the previously assigned critical role in neutrophil development[33]. Fluorescence-activated cell sorting (FACS) analysis confirmed that KLF6-, RUNX1- and RFX2-deficient cells generated a lower percentage of fully mature (Ly6G^{hi}CD101^{+}) neutrophils (Extended Data Fig. 5b). *Klf6*$^{-/-}$, *Runx1*$^{-/-}$ and *Rfx2*$^{-/-}$ also expressed lower levels of CD101, a marker of mature neutrophils[2], than (WT) cells (Fig. 3c).

Expression of primary granule enzyme myeloperoxidase (MPO) is downregulated during neutrophil maturation[2]. We observed the same trend in WT but not *Klf6*$^{-/-}$, *Runx1*$^{-/-}$ HoxB8 cells, where MPO levels remained high (Extended Data Fig. 5c). A hallmark of neutrophil terminal maturation is segmentation of the nucleus. Lamin-B2 (LMNB2) is considered important in the lobulation of the nucleus and is a predominant lamin in mature neutrophils[36]. Indeed, levels of LMNB2 steadily increased from day 1 to day 5 of HoxB8 WT differentiation and reached maximum at day 4/day 5 but remained low in *Klf6*$^{-/-}$ and *Runx1*$^{-/-}$ cells (Fig. 3d).

Another feature of neutrophil maturation is the decrease in their mitochondrial activity. Mature neutrophils possess a limited number of mitochondria and are defective in ATP production[37]. Indeed, mitochondrial membrane potential (MMP), a key indicator of mitochondrial activity and the driving force behind ATP production, was significantly lower in day 5, compared to day 3 HoxB8 neutrophils (Extended Data Fig. 5d). Consistent with their arrested maturation, *Klf6*$^{-/-}$ and *Runx1*$^{-/-}$ neutrophils displayed higher MMP (Extended Data Fig. 5d) compared to WT cells. Interestingly, deletion of JUNB also led to higher MMP, without affecting neutrophil maturation (Fig. 3a,b and Extended Data Fig. 5d). To further investigate a possible impact of selected transcription factors on the metabolic aspects of neutrophil development, we utilized the Seahorse assay to measure the oxygen consumption rate (OCR) as a key indicator of mitochondrial respiration (Supplementary Fig. 1). *Klf6*$^{-/-}$ or *Runx1*$^{-/-}$ neutrophils displayed higher levels of mitochondrial basal respiration, ATP turnover and mitochondrial maximal and spare capacities compared to WT cells (Fig. 3e). Other mutants had little impact on neutrophil mitochondrial activity, with the exception of *Rfx2*$^{-/-}$, which on average displayed a lower level in all metabolic measurements (Fig. 3e). We examined if RFX2 deficiency may lead to spontaneous apoptosis, using annexin V staining, and observed a dramatic increase in apoptotic rate compared to WT (Extended Data Fig. 5e). Deficiency in RELB also led to an increase in neutrophil apoptosis, which is consistent with the known function of NF-κB in supporting neutrophil survival and blocking spontaneous apoptosis[38].

Akin to findings in the HoxB8 system in vitro, conditional deletion of *Runx1* in myeloid populations produced a lower percentage (Fig. 3f) and absolute counts (Extended Data Fig. 6c) of Ly6G^{hi} CD101^{+} mature neutrophils in the bone marrow of naive *Lyz2*$^{Cre/Cre}$ × *Runx1*$^{loxP/loxP}$ mice, whereas no significant difference was observed in either *Irf5*$^{-/-}$ mice or *S100a8*^{Cre} × *JunB*$^{loxP/loxP}$ mice, with conditional deletion of *JunB* in neutrophils (Extended Data Fig. 6a,b). Corresponding percentages of immature Ly6G^{hi} CD101^{-} and c-Kit^{+}CXCR4^{+} preneutrophils were increased in the bone marrow of naive *Lyz2*$^{Cre/Cre}$ × *Runx1*$^{loxP/loxP}$ mice (Fig. 3f). Morphological characterization revealed a significantly lower percentage of segmented neutrophils and increased number of metamyelocyte-like cells in the bone marrow of *Lyz2*$^{Cre/Cre}$ × *Runx1*$^{loxP/loxP}$ (Extended Data Fig. 6d) but not *S100a8*^{Cre} × *JunB*$^{loxP/loxP}$ mice (Extended Data Fig. 6e). We investigated dependence of known neutrophil transcription factor expression on RUNX1 and found that expression of *Cebpe* was significantly reduced in *Runx1*$^{-/-}$ neutrophils (Fig. 3g), which is reminiscent of human data[39]. Furthermore, CEBPε protein levels were significantly reduced in bone marrow neutrophils of *Lyz2*$^{Cre/Cre}$ × *Runx1*$^{loxP/loxP}$ mice (Extended Data Fig. 6f). Expression of *Klf6* was independent of RUNX1 (Fig. 3g).

Thus, KLF6 and RUNX1, associated with neutrophil chromatin closing en route to the tissue, are independently involved in neutrophil maturation. RFX2 and RELB, linked to chromatin opening, support neutrophil survival.

RUNX1 and KLF6 deficiency impairs neutrophil recruitment. Neutrophil precursors display reduced migratory capacity in tissue[2]. We hypothesized that KLF6- and RUNX1-deficient neutrophils may display impaired (trans)migration properties. Using the Boyden chamber migration assay, we observed a significant reduction in the migration of day 5 *Runx1*$^{-/-}$ and *Klf6*$^{-/-}$ neutrophils, which was comparable to day 3 WT HoxB8 neutrophils (Fig. 4a).

To assess the impact of RUNX1 and KLF6 on the transcriptional programs involved in neutrophil maturation and migration, we performed mRNA-seq analysis of WT Hoxb8 neutrophils at days 0, 1, 3 and 5 and of *Runx1*$^{-/-}$ and *Klf6*$^{-/-}$ neutrophils at day 5. A total of 3,306 and 2,611 genes were differentially expressed in *Runx1*$^{-/-}$ and *Klf6*$^{-/-}$ neutrophils compared to day 5 WT cells, respectively. Hierarchical clustering of the DEGs identified five clusters, which encompassed genes downregulated (clusters 1 and 4) or upregulated with maturation (clusters 2, 3 and 5). Genes in clusters 2 and 5 were downregulated in *Runx1*$^{-/-}$ or *Klf6*$^{-/-}$ neutrophils, respectively (Extended Data Fig. 7a). GO annotation analysis revealed that these two clusters encompassed transcriptional programs of immune responses, cytokine production and leukocyte migration (Extended Data Fig. 7b). Genes in clusters 4 and 3 were upregulated in *Runx1*$^{-/-}$ or *Klf6*$^{-/-}$ neutrophils, respectively, with programs capturing metabolic and biosynthetic processes (Extended Data Fig. 7b). RUNX1 and KLF6 controlled a significant number of genes involved in leukocyte migration, such as important cell adhesion and chemotaxis molecules, including *Cxcr2*, *Sell*, *S100a8* or *Itgal*

Fig. 5 | RELB, IRF5 and JUNB control the immune responses of neutrophils. a, Putative target genes for each transcription factor: DEGs (HoxB8 WT versus transcription factor knockout in zymosan-induced HoxB8 neutrophils, $P_{adj} < 0.05$, fold change > 2) stratified by the identified binding sites for the corresponding transcription factors (FIMO $P < 0.0001$) within differentially accessible ATAC-seq peaks ($P_{adj} < 0.05$, fold change > 1.5) in the gene vicinity. **b**, GO biological process terms enriched for putative target genes as in **a**. **c**, CAV1 expression in HoxB8 neutrophils. Top: One representative western blot probed with antibodies specific for CAV1 and β-actin is shown. Bottom: Statistical analysis of CAV1 expression normalized against the amount of β-actin in the lysates (and expressed as the arbitrary unit of CAV1). Data are shown as the mean and s.d. from three independent experiments. Significant differences compared with the unstimulated WT neutrophils are denoted as $^{*}P < 0.05$, $^{**}P < 0.01$ (ordinary one-way ANOVA with Dunnett's multiple comparisons test). **d**, Phagocytosis of fluorescein-conjugated *E. coli* by WT and indicated knockout HoxB8 neutrophils, measured by flow cytometry. **e**, Intracellular ROS production by WT and indicated knockout HoxB8 neutrophils. **f**, Bacterial killing by HoxB8 neutrophils incubated with *Staphylococcus aureus* for 90 min before cell lysis. Values represent absolute CFU counts generated by surviving bacteria. Data are shown as the mean and s.d. derived from four independent experiments. **g**, NET formation in response to stimulation by PMA/ionomycin in WT and indicated knockout HoxB8 neutrophils. Data are expressed as the percentages of neutrophils undergoing NETosis out of at least 200 cells counted from different fields and independent replicates. Data are shown as the mean and s.d. derived from three independent experiments. **d**,**e**,**g**, Significant differences between knockout and WT neutrophils are denoted as $^{*}P < 0.05$, $^{**}P < 0.01$, $^{****}P < 0.0001$ (repeated measures one-way ANOVA with Dunnett's multiple comparisons test).

for RUNX1 and *Vcam1*, *Cd9*, *C3ar1*, *Cx3cr1* and *Icam1* for KLF6 (Extended Data Fig. 7c).

To examine the role of selected transcription factors in neutrophil recruitment in vivo, we injected intravenously an equal mix of CellTracker Far Red–labeled WT and CellTracker carboxyfluorescein succinimidyl ester (CFSE)–labeled knockout HoxB8 neutrophils into the air pouch cavity (Fig. 4b). The recruitment of WT and knockout cells was monitored at 4 h postzymosan injection

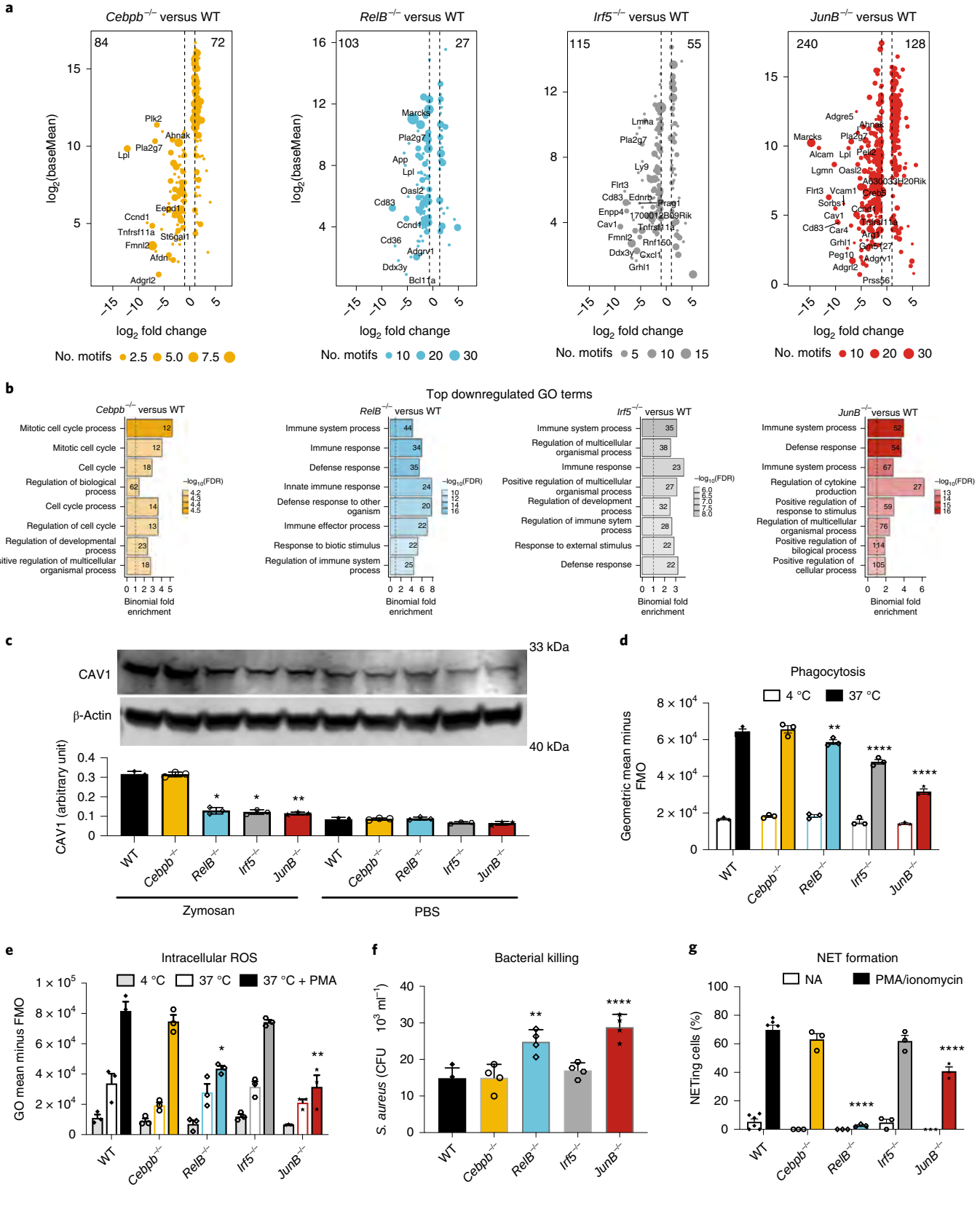

(Supplementary Fig. 2). We observed reduced infiltration of *Klf6*$^{-/-}$ *Runx1*$^{-/-}$ and *Rfx2*$^{-/-}$ HoxB8 neutrophils into the sites of inflammation, while the recruitment of *C/ebpβ*$^{-/-}$, *RelB*$^{-/-}$, *Irf5*$^{-/-}$ and *JunB*$^{-/-}$ HoxB8 neutrophils was unaffected (Fig. 4c). Deficiency in RELB and RFX2, which has been shown to accelerate neutrophil apoptosis at steady state (Extended Data Fig. 5e), also limited neutrophil survival during inflammation, with RFX2 showing the strongest effect in all compartments (Extended Data Fig. 7d).

When *Lyz2*$^{Cre/Cre}$ × *Runx1*$^{loxP/loxP}$ and control *Runx1*$^{loxP/loxP}$ mice were subjected to the air pouch model, zymosan induction led to depletion of mature neutrophils in the bone marrow and stimulated egress of immature neutrophils into the circulation (Extended Data Figs. 7e and 1g,h), with a shift toward fewer mature neutrophils and a trend toward a higher number of immature neutrophils in the blood of *Lyz2*$^{Cre/Cre}$ × *Runx1*$^{loxP/loxP}$ mice (Extended Data Fig. 7e). The total number of neutrophils in circulation was comparable between the genotypes but the number of neutrophils mobilized into the site of inflammation was significantly lower in the *Lyz2*$^{Cre/Cre}$ *xRunx1*$^{loxP/loxP}$ mice (Fig. 4d), most likely attributed to fewer circulating mature neutrophils (Extended Data Fig. 7e).

In summary, our data place KLF6 and RUNX1 at the apex of the neutrophil differentiation cascade, where they may independently control multiple associated processes, including neutrophil segmentation, migration, granular content and metabolism.

RELB, IRF5 and JUNB control neutrophil activation and effector functions. Next, we investigated whether transcription factors associated with chromatin opening, expressed more highly in circulating, activated and tissue neutrophils, and not implicated in neutrophil development (C/EBPβ, RELB, IRF5, JUNB) regulated neutrophil activation. We conducted mRNA-seq analysis of WT and transcription factor–deficient HoxB8 neutrophils challenged with zymosan for 2 h. Expression of 4,887 genes was affected in WT cells by zymosan stimulation; 2,914, 3,047, 3,691 and 6,292 genes were differentially expressed in *Cebpb*$^{-/-}$, *RelB*$^{-/-}$, *Irf5*$^{-/-}$ or *JunB*$^{-/-}$ zymosan-stimulated neutrophils compared to corresponding WT cells, respectively (Extended Data Fig. 8a). GO annotation analysis of global gene expression revealed the role for RELB, IRF5 and JunB in the regulation of zymosan-induced immune genes and pathways, as well as contribution to zymosan-independent cellular processes, for example, DNA recombination and replication or ribosome biosynthesis (Extended Data Fig. 8b). Since both direct and indirect targets of selected transcription factors contribute to the DEG pool, we attempted to define putative 'target genes' for each transcription factor. First, we searched for consensus transcription factor binding motifs in the regions of open chromatin identified by ATAC-Seq (Fig. 2). Then, we selected genes proximal to these motifs. Lastly, we intersected these genes with the DEG for a corresponding transcription factor knockout in stimulated Hoxb8 neutrophils (Extended Data Fig. 8a) and found that JUNB appeared to control the highest number of target genes, whereas RELB, IRF5 and CEBPβ had a more limited impact (Fig. 5a). GO annotation analyses revealed that JUNB, RELB and IRF5 were likely to control immune genes and categories, while C/EBPβ was most likely involved in the regulation of cellular processes (Fig. 5b). For example, calveolin 1 (*Cav1*), a gene target for both IRF5 and JUNB (Fig. 5a), is involved in neutrophil activation, adhesion and transendothelial migration[40]. We confirmed that CAV1 protein expression was significantly diminished in *RelB*$^{-/-}$, *Irf5*$^{-/-}$ or *JunB*$^{-/-}$ but not *Cebpb*$^{-/-}$ zymosan-stimulated neutrophils (Fig. 5c).

To validate the importance of selected transcription factors in neutrophil activation, we examined the consequence of their knockout on neutrophil effector functions[2]. IRF5 and JUNB deficiency affected the ability of neutrophils to phagocytose bacteria (Fig. 5d), while RELB and JUNB were important for ROS production (Fig. 5e), bacterial killing (Fig. 5f) and neutrophil extracellular trap (NET) formation (Fig. 5g and Extended Data Fig. 8c). This was supported by decreased expression of key genes involved in ROS generation and phagocytosis (Extended Data Fig. 8d,e). For example, RELB was required for the expression of *Cyba* and *Ncf1*, two components of the NADPH oxidase complex (Extended Data Fig. 8d). JUNB had the strongest effect on genes involved in phagocytosis, such as *Cd302*, *Icam5*, *Itgb* and *Tgm2* (Extended Data Fig. 8e).

Thus, among the transcription factors active in the blood-to-tissue transition, JUNB demonstrated the most consistent overall effect on neutrophil effector functions, while the contributions of IRF5 and RELB were more nuanced and that of C/EBPβ was minimal.

RELB, IRF5 and JUNB control the expression of inflammatory mediators. Expression of cytokines and chemokines by HoxB8 neutrophils was strongly and globally upregulated in response to zymosan treatment and affected by RELB, IRF5 and JUNB deficiency (Extended Data Fig. 9a,b). Zooming in, we observed a significant reduction in mRNA expression of the pro-inflammatory cytokines *Il1a*, *Il1β*, *Tnf* and *Il6* and the chemokines *Ccl2* and *Cxcl2* in zymosan-stimulated *RelB*$^{-/-}$, *Irf5*$^{-/-}$ or *JunB*$^{-/-}$ cells (Fig. 6a and Extended Data Fig. 9c). Impaired mRNA expression led to reduced protein production, measured by multiplex antibody array (Extended Data Fig. 9d). After a 15-min (short) exposure, we detected CCL2, CCL3, CCL4, CXCL2, CXCL10, TNF and IL-1ra (Fig. 6b). *RelB*$^{-/-}$cells displayed reduced levels of CCL2, IL-1ra, TNF and CXCL10; *Irf5*$^{-/-}$ cells displayed reduced levels of IL-1ra and TNF (Fig. 6b). Once again, deficiency in JUNB affected the widest range of mediators (Fig. 6b). After a 30-min (long) exposure, we detected a significant decrease in the secretion of IL-1B by *RelB*$^{-/-}$, *Irf5*$^{-/-}$ and *JunB*$^{-/-}$ HoxB8 neutrophils in comparison to WT cells (Extended Data Fig. 9e), which was mirrored by a decrease in pro-IL-1B expression (Fig. 6c).

Fig. 6 | RELB, IRF5 and JUNB deficiency impairs neutrophil inflammatory responses. a, *Il1b*, *Tnf* and *Ccl2* mRNA induction in HoxB8 neutrophils stimulated with zymosan (50 μg ml^{-1}) for 0, 1 and 2 h. Gene expression was measured by quantitative PCR with reverse transcription. Data are shown as the mean and s.d. from three independent experiments. **b**, Cytokine and chemokine production of HoxB8 neutrophils stimulated with zymosan (50 μg ml^{-1}) for 2 h. Cytokines and chemokines secreted into the supernatant were measured by proteome array. The results are shown as the mean and s.d. from three biologically independent samples. **a**,**b**, Significant differences between knockout and WT neutrophils are denoted as $^{*}P < 0.05$, $^{**}P < 0.01$, $^{***}P < 0.001$ and $^{****}P < 0.0001$ (repeated measures one-way ANOVA with Dunnett's multiple comparisons test). **c**, Pro-IL-1β production by HoxB8 neutrophils stimulated with zymosan (50 μg ml^{-1}) for 2 h assessed by intracellular flow cytometry staining. Data are shown as the mean and s.d. derived from three independent experiments. Significant differences between knockout and WT neutrophils are denoted as $^{**}P < 0.01$, $^{****}P < 0.0001$ and NS (ordinary one-way ANOVA with Dunnett's multiple comparisons test). **d**, Experimental setup of differentially labeled WT and transcription factor knockout HoxB8 neutrophils adoptively transferred into the air pouch model of acute inflammation; the activation of neutrophils was assessed by pro-IL-1β expression. **e**, Expression of pro-IL-1β, as measured by flow cytometry, in HoxB8 neutrophils recovered from the bone marrow, blood, air pouch membrane and air pouch exudate of mice subjected to the air pouch model and zymosan challenge. Data are shown as the mean and s.d. from 4–6 mice in one experiment. **f**, Experimental setup (left) and pro-IL-1β production (right) by neutrophils in *Irf5*$^{loxP/loxP}$ or *S100a8*^{Cre}*Irf5*$^{loxP/loxP}$ mice subjected to the air pouch model and zymosan challenge. Data are shown as the mean and s.d. from five mice. **e**,**f**, Significant differences between *Irf5*$^{loxP/loxP}$ and *S100a8*^{Cre}*Irf5*$^{loxP/loxP}$ mice are denoted as $^{*}P < 0.05$ and $^{****}P < 0.0001$ (repeated measures two-way ANOVA with Šidák's multiple comparisons test).

We used an adoptive HoxB8 neutrophil transfer into the air pouch model (Fig. 4c) to examine the effect of transcription factor knockout on neutrophil ability to produce inflammatory mediators in vivo (Fig. 6d). *RelB*$^{-/-}$, *Irf5*$^{-/-}$ or *JunB*$^{-/-}$ HoxB8 neutrophils in the membrane and/or exudate produced less pro-IL-1β than WT neutrophils (Fig. 6e). When mice with conditional deletion of *Irf5* in neutrophils, *S100a8*^{Cre}*xIrf5*$^{loxP/loxP}$, were subjected to the air pouch model, IRF5-deficient neutrophils displayed a significant reduction in pro-IL-1β at the site of inflammation (Fig. 6f), matching the adoptive transfer experiments (Fig. 6e).

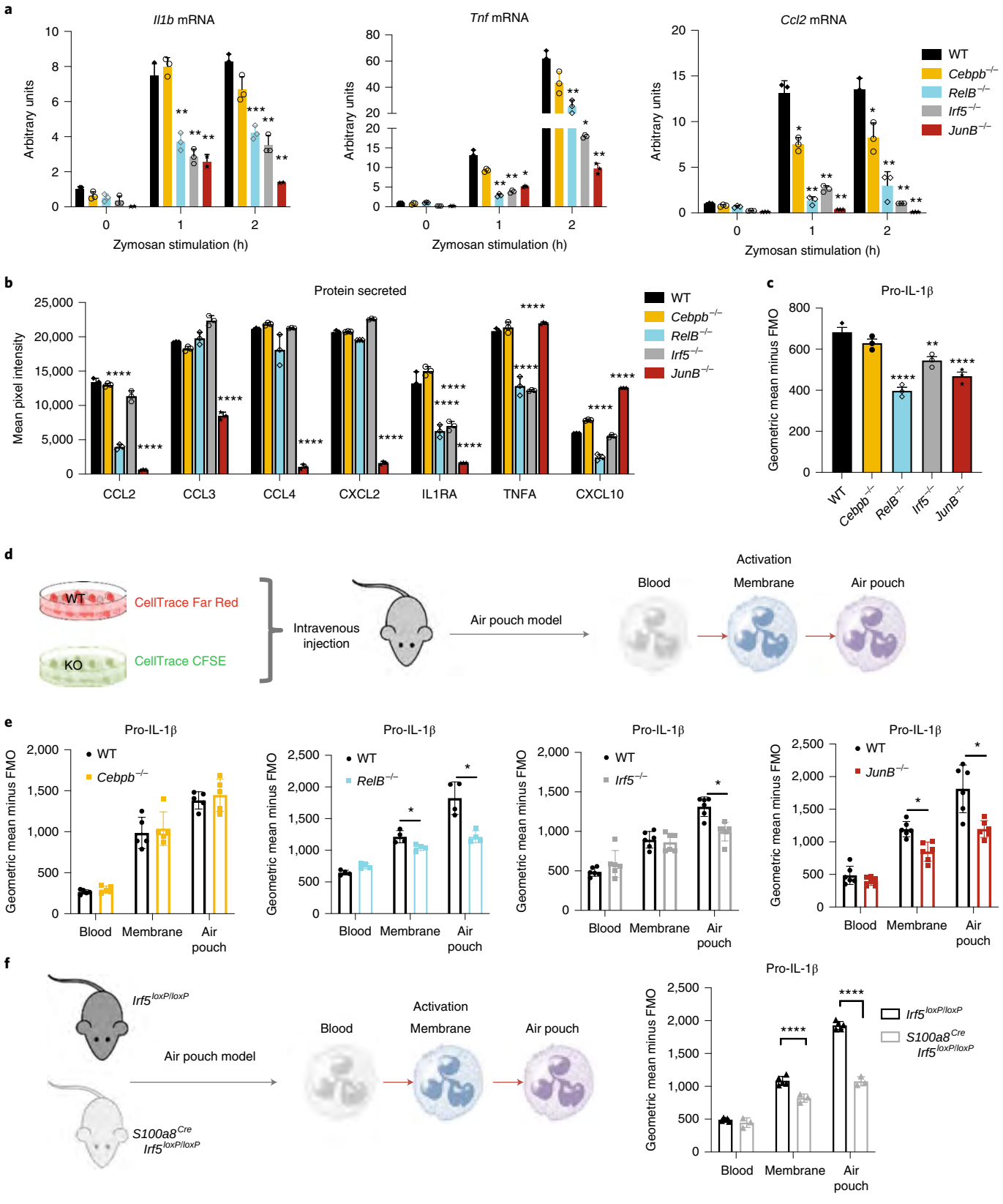

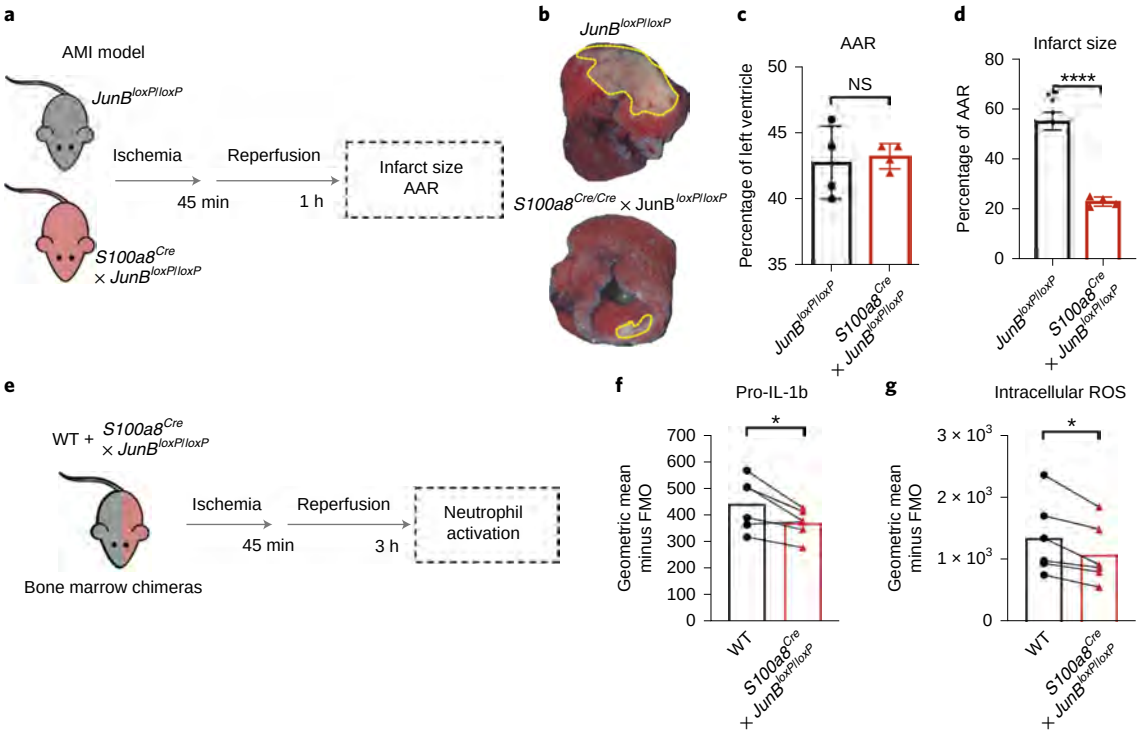

Fig. 7 | Neutrophil-specific knockout of *JunB* limits pathological destruction of tissue during neutrophil-driven inflammation. a, Mouse model of AMI. The left anterior descending coronary artery was occluded for 45 min; this was followed by reperfusion for 1 h. **b**, Representative images of heart slices stained with TTC and normalized to area at risk (AAR; negative Evans blue staining) from $JunB^{loxP/loxP}$ and $S100a8^{Cre/Cre} \times JunB^{loxP/loxP}$ mice subjected to ischemia-reperfusion injury. The dotted yellow lines highlight areas of dead myocardium. **c**,**d**, Histological evaluation of the left ventricle AAR (**c**) and infarct size (**d**) in mice subjected to ischemia-reperfusion injury. All results are shown as the mean and s.d. derived from four mice from each group in one experiment. Significant differences between $JunB^{loxP/loxP}$ and $S100a8^{Cre/Cre} \times JunB^{loxP/loxP}$ mice were determined by unpaired Student's *t*-test analysis. $^{****}P < 0.0001$ and NS. **e**, Mixed bone marrow chimera setup to measure neutrophil activation in the shared inflammatory environment of AMI. **f**,**g**, Production of pro-IL-1b (**f**) or ROS (**g**) as measured by flow cytometry in WT and JUNB-deficient neutrophils in mixed bone marrow chimera mice subjected to permanent myocardial infarction. Data are shown as the mean and s.d. derived from three mice from each group in one experiment. Statistical comparison was made by paired Student's *t*-test; $^{*}P < 0.05$.

Finally, we sought to demonstrate that interference with neutrophil activation would curb pathological inflammation in vivo by applying a neutrophil-dependent model of acute myocardial infarction (AMI) induced by ischemia-reperfusion of the left anterior descending coronary artery[6] to $S100a8^{Cre} \times JunB^{loxP/loxP}$ mice (Fig. 7a). The analysis revealed a significant reduction in infarct size in mice with neutrophil-specific ablation of JunB compared to littermate controls (Fig. 7b–d). To examine whether JUNB intrinsically controls neutrophil activation at inflamed sites, we generated mixed chimeric mice harboring both control and JUNB-deficient ($S100a8^{Cre} \times JunB^{loxP/loxP}$) neutrophils by bone marrow transplantation into WT recipient mice; 3 h after induction of cardiac ischemia-reperfusion injury, we analyzed neutrophils in the myocardia (Fig. 7e) and confirmed no substantial change in the chimerism ratio in bone marrow:blood or blood:heart transitions (Extended Data Fig. 10a), thereby corroborating our finding that neutrophil recruitment to the site of inflammation is not affected by depletion of JUNB in neutrophils (Fig. 4c). In agreement with our in vitro and in vivo analyses (Figs. 5e and 6c,e), we found consistent reductions in the levels of pro-IL-1b (Fig. 7f) and intracellular ROS (Fig. 7g) in JUNB-deficient neutrophils compared to their WT counterparts.

Together, these data suggest that IRF5, RELB and JUNB have limited roles in neutrophil maturation but significantly regulate inflammatory cytokines production in vitro and at the sites of inflammation in vivo. Moreover, neutrophil-specific inhibition of JUNB limits pathological destruction of tissue during neutrophil-driven inflammation (Extended Data Fig. 10b).

Discussion

It is becoming increasingly clear that neutrophils, which have previously been considered as transcriptionally inactive cells, display distinct gene expression profiles at different developmental stages[2], activation states[9] and microenvironments[41,42]. Nevertheless, the transcriptional networks that shape neutrophil function have not yet been defined. In this study, we investigated the transcriptional and chromatin landscape of neutrophils during sterile inflammation and identified previously unappreciated transition points in neutrophil transcriptional regulation, from bone marrow to the blood and from the blood to the tissue, each associated with the involvement of a distinct set of transcription factors. Further functional validation of candidate transcription factors in vitro and in vivo, dissociated cell state-specific transcription factors that modulate neutrophil maturation (RUNX1, KLF6) from transcription factors driving neutrophil effector responses (RELB, IRF5, JUNB) and/or neutrophil survival (RFX2, RELB), thus opening new possibilities for specific stage-specific modulation of neutrophil function in disease.

The capture of transcriptional changes related to neutrophil maturation at the transition from bone marrow to the blood likely reflects differences in proportion of immature $Ly6G^{+}CD101^{-}$ and mature $Ly6G^{+}CD101^{+}$ neutrophils in the bone marrow and blood samples, which is consistent with recently published studies[2,11].

Genomic and transcriptomic differences separating bone marrow and blood neutrophils may in part be the reason for a long held view on immaturity of mouse neutrophils and their differences with human neutrophils[11,22,43,44] since most of mouse studies focused on bone marrow neutrophils and most human studies used blood neutrophils. This highlights the need for careful consideration of the experimental source of cells in neutrophil studies.

In differentially accessible chromatin regions between the bone marrow and blood, we identified binding motifs for transcription factors, such as RUNX1 and KLF6, which facilitate neutrophil maturation. RUNX1 is a transcription factor with a major role in myelopoiesis; it promotes neutrophil terminal differentiation in a *Cebpe*-dependent manner[39], which we confirmed in this study. KLF6 is a transcription factor linked to the pathogenesis of acute myeloid leukemia[45]; its role in neutrophil maturation has not been previously addressed. Differentiating neutrophils undergo a metabolic reprogramming toward glycolysis on maturation[46], which ensures that neutrophils can function in an inflammatory environment where the oxygen tension may be low or even absent[47,48]. At the same time, we and others observed the decrease in their mitochondrial activity during the final stages of neutrophil maturation. In line with their immature phenotype, KLF6- and RUNX1-deficient neutrophils display higher mitochondrial membrane potential, which is associated with respiratory chain activity and oxidative phosphorylation. They are also characterized by a higher level of mitochondrial basal respiration, ATP turnover and mitochondrial maximal and spare capacities compared to WT. Another consequence of neutrophil maturation is their ability to rapidly migrate toward sites of inflammation[2,22]. Indeed, neutrophils deficient in RUNX1 or KLF6 could not efficiently reach the site of inflammation. RNA-seq analysis confirmed that these transcription factors positively control transcriptional programs upregulated with maturation, such as immune responses or leukocyte migration, but also inhibit programs related to metabolic and biosynthetic processes. Further mapping of transcriptional control of neutrophil differentiation trajectory and functional validation of the transcription factors involved would provide new insights into the current model of neutrophil development. scRNA-seq profiling of neutrophils[2,11] is the essential basis for such analysis, while emerging spatial genomics technologies would help to avoid the impact of cell isolation.

Importantly, factors regulating the transition from blood into the tissue (IRF5, JUNB and RELB) do not affect respiration and mitochondrial function of neutrophils, nor do they impair their migration into the tissue. Instead, they contribute to cytokine and chemokine expression and production and various effector functions, such as phagocytosis, generation of ROS, bacterial killing or NETosis. JUNB demonstrated the strongest overall effect on neutrophil effector functions, which is consistent with the previously reported role of JUNB in setting up the neutrophil inflammatory response[49]. Neutrophil-specific ablation of JUNB has a profound effect on the extent of infarct in the model of AMI, supporting the notion that neutrophil transcriptional reprogramming could offer alternative therapeutic strategies to manage cardiovascular disease. As highlighted previously[9], IRF5 plays a role in regulating inflammatory gene expression but also contributes to regulation of neutrophil phagocytosis, while its involvement in ROS production and NETosis is limited. On the contrary, RELB is critical for the formation of NETs and drives ROS production via expression of specific subunits of the catalytic NOX2 complex of NADPH. RELA, another member of the NF-kB family, has also been implicated in ROS induction in myeloid cells via different NADPH complex subunits[50], raising the possibility for their coordinated action.

RFX2 and RELB are critical for neutrophil survival at the steady state and during inflammation. While the role of the NF-κB family in supporting neutrophil survival and blocking spontaneous apoptosis has been documented previously[38], the pro-survival function of RFX2 in immune cells has not been described previously. RFX2-deficient mice do not have an obvious embryonic phenotype but absence of RFX2 results in germ cell apoptosis[51], suggesting a general role for RFX2 in controlling cell survival across cell lineages. Considering high levels of RFX2 expression in neutrophils compared to other immune cells, it will be important to examine how *Rfx2*$^{-/-}$ mice control infection and inflammation.

In summary, our study provides a significant advance in understanding the molecular mechanisms underlining neutrophil development and function during inflammation by depicting key transcription factor modules that modulate development versus inflammatory responses or survival. It extends our understanding of neutrophil transcriptional reprogramming from adaptation to local tissue environment at homeostasis[13], to acquisition of specific effector functions under inflammation. We generated the first draft of the neutrophil transcriptional blueprint in the context of in vivo inflammation, which will undoubtedly be edited and filled in with more details in the future. Moreover, the distinct repertoires of transcription factors controlling neutrophil maturation and activation may lead to multiple therapeutic strategies tailored to specific conditions. For example, stimulation of neutrophil maturation may be beneficial for postchemotherapy cancer patients. Inhibition of neutrophil activation, in contrast, may help to reduce the inflammatory burden suffered during inflammation-associated diseases, such as cardiovascular diseases. Induction of neutrophil effector functions may be needed in infectious diseases and early stages of cancer.

Online content

Any methods, additional references, Nature Research reporting summaries, source data, extended data, supplementary information, acknowledgements, peer review information; details of author contributions and competing interests; and statements of data and code availability are available at https://doi.org/10.1038/s41590-021-00968-4.

Received: 27 November 2020; Accepted: 4 June 2021;
Published online: 19 July 2021

References

1. Cowland, J. B. & Borregaard, N. Granulopoiesis and granules of human neutrophils. *Immunological Rev.* **273**, 11–28 (2016).
2. Evrard, M. et al. Developmental analysis of bone marrow neutrophils reveals populations specialized in expansion, trafficking, and effector functions. *Immunity* **48**, 364–379.e8 (2018).
3. Lawrence, S. M., Corriden, R. & Nizet, V. The ontogeny of a neutrophil: mechanisms of granulopoiesis and homeostasis. *Microbiol. Mol. Biol. Rev.* **82**, e00057-17 (2018).
4. Nauseef, W. M. & Borregaard, N. Neutrophils at work. *Nat. Immunol.* **15**, 602–611 (2014).
5. Scapini, P. & Cassatella, M. A. Social networking of human neutrophils within the immune system. *Blood* **124**, 710–719 (2014).
6. Adrover, J. M. et al. A neutrophil timer coordinates immune defense and vascular protection. *Immunity* **50**, 390–402.e10 (2019).
7. Beyrau, M., Bodkin, J. V. & Nourshargh, S. Neutrophil heterogeneity in health and disease: a revitalized avenue in inflammation and immunity. *Open Biol.* **2**, 120134 (2012).
8. Silvestre-Roig, C., Hidalgo, A. & Soehnlein, O. Neutrophil heterogeneity: implications for homeostasis and pathogenesis. *Blood* **127**, 2173–2181 (2016).
9. Ericson, J. A. et al. Gene expression during the generation and activation of mouse neutrophils: implication of novel functional and regulatory pathways. *PLoS ONE* **9**, e108553 (2014).
10. Ostuni, R., Natoli, G., Cassatella, M. A. & Tamassia, N. Epigenetic regulation of neutrophil development and function. *Semin. Immunol.* **28**, 83–93 (2016).
11. Xie, X. et al. Single-cell transcriptome profiling reveals neutrophil heterogeneity in homeostasis and infection. *Nat. Immunol.* **21**, 1119–1133 (2020).
12. Zhu, Y. et al. Comprehensive characterization of neutrophil genome topology. *Genes Dev.* **31**, 141–153 (2017).
13. Ballesteros, I. et al. Co-option of neutrophil fates by tissue environments. *Cell* **183**, 1282–1297.e18 (2020).

14. Kolaczkowska, E. & Kubes, P. Neutrophil recruitment and function in health and inflammation. *Nat. Rev. Immunol.* **13**, 159–175 (2013).
15. Sagiv, J. Y., Voels, S. & Granot, Z. Isolation and characterization of low- vs. high-density neutrophils in cancer. *Methods Mol. Biol.* **1458**, 179–193 (2016).
16. Yvan-Charvet, L. & Ng, L. G. Granulopoiesis and neutrophil homeostasis: a metabolic, daily balancing act. *Trends Immunol.* **40**, 598–612 (2019).
17. Hohaus, S. et al. PU. 1 (Spi-1) and C/EBP alpha regulate expression of the granulocyte-macrophage colony-stimulating factor receptor alpha gene. *Mol. Cell. Biol.* **15**, 5830–5845 (1995).
18. Nerlov, C. & Graf, T. PU. 1 induces myeloid lineage commitment in multipotent hematopoietic progenitors. *Genes Dev.* **12**, 2403–2412 (1998).
19. Hock, H. et al. Intrinsic requirement for zinc finger transcription factor Gfi-1 in neutrophil differentiation. *Immunity* **18**, 109–120 (2003).
20. Yamanaka, R. et al. Impaired granulopoiesis, myelodysplasia, and early lethality in CCAAT/enhancer binding protein ε-deficient mice. *Proc. Natl Acad. Sci. USA* **94**, 13187–13192 (1997).
21. Ai, Z. & Udalova, I. A. Transcriptional regulation of neutrophil differentiation and function during inflammation. *J. Leukoc. Biol.* **107**, 419–430 (2020).
22. Grassi, L. et al. Dynamics of transcription regulation in human bone marrow myeloid differentiation to mature blood neutrophils. *Cell Rep.* **24**, 2784–2794 (2018).
23. Jarvis, J. N. et al. Gene expression profiling in neutrophils from children with polyarticular juvenile idiopathic arthritis. *Arthritis Rheum.* **60**, 1488–1495 (2009).
24. Cloutier, A. et al. Inflammatory cytokine production by human neutrophils involves C/EBP transcription factors. *J. Immunol.* **182**, 563–571 (2009).
25. Tessier, P. A. et al. Chemokine networks in vivo: involvement of C-X-C and C-C chemokines in neutrophil extravasation in vivo in response to TNF-alpha. *J. Immunol.* **159**, 3595–3602 (1997).
26. Harris, J. G., Flower, R. J. & Perretti, M. Endogenous corticosteroids mediate the neutrophilia caused by platelet-activating factor in the mouse. *Eur. J. Pharmacol.* **283**, 9–18 (1995).
27. Ryckman, C. et al. Role of S100A8 and S100A9 in neutrophil recruitment in response to monosodium urate monohydrate crystals in the air-pouch model of acute gouty arthritis. *Arthritis Rheum.* **48**, 2310–2320 (2003).
28. Wilkinson, L. S., Moore, A. R., Pitsillides, A. A., Willoughby, D. A. & Edwards, J. C. Comparison of surface fibroblastic cells in subcutaneous air pouch and synovial lining: differences in uridine diphosphoglucose dehydrogenase activity. *Int. J. Exp. Pathol.* **74**, 113–115 (1993).
29. Blazek, K. et al. IFN-λ resolves inflammation via suppression of neutrophil infiltration and IL-1β production. *J. Exp. Med.* **212**, 845–853 (2015).
30. Monticelli, S. & Natoli, G. Transcriptional determination and functional specificity of myeloid cells: making sense of diversity. *Nat. Rev. Immunol.* **17**, 595–607 (2017).
31. Jojic, V. et al. Identification of transcriptional regulators in the mouse immune system. *Nat. Immunol.* **14**, 633–643 (2013).
32. Hirai, H. et al. C/EBPβ is required for 'emergency' granulopoiesis. *Nat. Immunol.* **7**, 732–739 (2006).
33. Paul, F. et al. Transcriptional heterogeneity and lineage commitment in myeloid progenitors. *Cell* **163**, 1663–1677 (2015).
34. Wang, G. G. et al. Quantitative production of macrophages or neutrophils ex vivo using conditional Hoxb8. *Nat. Methods* **3**, 287–293 (2006).
35. Wang, L. et al. ROS producing immature neutrophils in giant cell arteritis are linked to vascular pathologies. *JCI Insight* **5**, e139163 (2020).
36. Manley, H. R., Keightley, M. C. & Lieschke, G. J. The neutrophil nucleus: an important influence on neutrophil migration and function. *Front. Immunol.* **9**, 2867 (2018).
37. van Raam, B. J. et al. Mitochondrial membrane potential in human neutrophils is maintained by complex III activity in the absence of supercomplex organisation. *PLoS ONE* **3**, e2013 (2008).
38. Ward, C. et al. NF-κB activation is a critical regulator of human granulocyte apoptosis in vitro. *J. Biol. Chem.* **274**, 4309–4318 (1999).
39. Ng, K. P. et al. Runx1 deficiency permits granulocyte lineage commitment but impairs subsequent maturation. *Oncogenesis* **2**, e78 (2013).
40. Hu, G., Ye, R. D., Dinauer, M. C., Malik, A. B. & Minshall, R. D. Neutrophil caveolin-1 expression contributes to mechanism of lung inflammation and injury. *Am. J. Physiol. Lung Cell. Mol. Physiol.* **294**, L178–L186 (2008).
41. Casanova-Acebes, M. et al. Rhythmic modulation of the hematopoietic niche through neutrophil clearance. *Cell* **153**, 1025–1035 (2013).
42. Sionov, R. V., Fridlender, Z. G. & Granot, Z. The multifaceted roles neutrophils play in the tumor microenvironment. *Cancer Microenviron.* **8**, 125–158 (2015).
43. Borregaard, N. Neutrophils, from marrow to microbes. *Immunity* **33**, 657–670 (2010).
44. Kwok, I. et al. Combinatorial single-cell analyses of granulocyte-monocyte progenitor heterogeneity reveals an early uni-potent neutrophil progenitor. *Immunity* **53**, 303–318.e5 (2020).
45. Humbert, M. et al. Deregulated expression of Kruppel-like factors in acute myeloid leukemia. *Leuk. Res.* **35**, 909–913 (2011).
46. Riffelmacher, T. et al. Autophagy-dependent generation of free fatty acids is critical for normal neutrophil differentiation. *Immunity* **47**, 466–480.e5 (2017).
47. Borregaard, N. & Herlin, T. Energy metabolism of human neutrophils during phagocytosis. *J. Clin. Invest.* **70**, 550–557 (1982).
48. Walmsley, S. R. et al. Hypoxia-induced neutrophil survival is mediated by HIF-1α–dependent NF-κB activity. *J. Exp. Med.* **201**, 105–115 (2005).
49. Fischer, J. et al. Safeguard function of PU.1 shapes the inflammatory epigenome of neutrophils. *Nat. Immunol.* **20**, 546–558 (2019).
50. Anrather, J., Racchumi, G. & Iadecola, C. NF-κB regulates phagocytic NADPH oxidase by inducing the expression of gp91*phox*. *J. Biol. Chem.* **281**, 5657–5667 (2006).
51. Wu, Y. et al. Transcription factor RFX2 is a key regulator of mouse spermiogenesis. *Sci. Rep.* **6**, 20435 (2016).
52. Picelli, S. et al. Full-length RNA-seq from single cells using Smart-seq2. *Nat. Protoc.* **9**, 171–181 (2014).

Methods

Materials and reagents. Details of commercially available reagents and other materials used in this study are summarized in Supplementary Table 1.

Air pouch model of acute inflammation. Mice were bred and maintained under specific pathogen-free conditions in accredited animal facilities at the University of Oxford and were housed in individually ventilated cages at a constant 20–23.3 °C with a 12 h dark–light cycle and supplied with food and water ad libitum. All experimental procedures were approved by the local animal care and ethics committees (Oxford and Madrid). Animal housing, handling and experimental procedures in Oxford were conducted under a UK Home Office Project licence to I.A.U. The air pouch model of acute inflammation was established as described previously[29]. Briefly, C57BL/6J male mice (Charles River Laboratories) were maintained at nine weeks of age and allowed to acclimatize for one week. Mice were anesthetized with isoflurane and 3 ml of air was injected subcutaneously to create a dorsal air pouch with a top-up of air 3 d later. At 5 d after the creation of the air pouch, mice were challenged with 1 mg of zymosan injected directly into the pouch. Challenged mice were culled after 1, 2, 4, 12 and 24 h after zymosan injection and bone marrow, blood, membrane and exudate were collected.

Cell and tissue preparation. Blood was obtained via cardiac puncture; then, red blood cells were lysed in ACK lysis buffer (Thermo Fisher Scientific). For bone marrow cells, mice femurs were flushed using a 23-G needle in PBS and passed through a 70-mm nylon mesh sieve. Membrane tissue was collected from mice and digested with 20 ml of Roswell Park Memorial Institute (RPMI) medium + 10% FCS + 1% PS (penicillin streptomycin) + 2.5 U ml^{-1} of collagenase type VIII (Sigma-Aldrich) + 2 U ml^{-1} of DNase I (Roche) and passed through a 70-mm nylon mesh sieve. Exudate was passed through a 70-mm nylon mesh sieve. Cells were pelleted by centrifugation at 400 rcf for 5 min before counting.

Flow cytometry and cell sorting. To identify preneutrophils, immature and mature neutrophils, cells were washed and preincubated with Fc Block (BD Biosciences) before surface staining with 1:200-diluted fluorophore-conjugated anti-mouse antibodies against CD11b (clone M1/70), cKit (clone 2B8), Ly6C (clone HK1.4), Ly6G (clone 1A8), CXCR2 (clone SA044G4), CXCR4 (clone 2B11) and CD101 (clone Moushi101), together with exclusion lineage markers that include CD3e (clone 145-2C11), B220 (clone RA3-6B2), NK.1.1 (clone PK136), Sca-1 (clone D7), CD11c (clone N418), CD19 (clone 6D5) and Siglec-F (clone E50-2440) (Supplementary Table 1). For surface staining, neutrophils were segregated into preneutrophils and immature and mature neutrophils (Supplementary Fig. 3). For intracellular cytokine staining, surface staining was followed by fixation and then permeabilization to allow for intracellular staining with pro–IL-1β (clone NJTEN3). Flow cytometry acquisition was performed using the FACSDiva v.6.1.3 software (on an LSR and LSRFortessa X-20; BD Biosciences). Data analysis was performed using FlowJo v.10 (FlowJo LLC).

RNA-seq analysis. Neutrophils from bone marrow, blood, membrane and exudate were sorted from CX3CR1GFP Ly6G^{Cre}-tdTomato mice subjected to air pouch of inflammation, based on the gating strategy depicted in Extended Data Fig. 1f. Three hundred cell samples were sorted through a 100-µm diameter nozzle into 2 µl of lysis buffer and amplified complementary DNA was prepared for small bulk RNA-seq using the Smart-seq2 protocol[52]. Libraries were prepared using Nextera XT kits (Illumina) and sequenced to a mean depth of 17 M read pairs (Illumina HiSeq 4000).

HoxB8 neutrophils differentiated for 5 d were incubated with zymosan (50 µg ml^{-1}) or dimethylsulfoxide (DMSO) vehicle for 2 h. Total RNA was extracted using the RNeasy Mini Kit (QIAGEN) according to the manufacturer's instructions. Subsequently, poly-A selected mRNA libraries were sequenced on an Illumina HiSeq 4000 yielding 20–30 × 10^6 150 base pair (bp) paired-end reads per sample. These were mapped to the mm10 genome using STAR v2.7.5b with the options: --runMode alignReads --outFilterMismatchNmax 2. Uniquely mapped read pairs were counted over annotated genes using featureCounts v.2.0.0 with the options: -T 18 -s 2 -Q 255. Differential expression was then analyzed with DESeq2 v1.24.0 (ref. [53]). Variance stabilized counts for all DESeq2 DEGs, likelihood ratio test and false discovery rate (FDR) <0.01 were used for dimensionality reduction and the heatmaps. GO analysis was performed using one-sided Fisher's exact tests, as implemented in the gsfisher v0.2 R package (https://github.com/sansomlab/gsfisher/). GSEA was performed using the fgsea R package v1.10.1.

ATAC-seq. ATAC-seq was performed using the published ATAC protocol[54]. Samples were quality-checked for ATAC-seq-specific patterning on a bioanalyzer chip and were pooled at an equimolar ratio and sequenced on a HiSeq 2500 using 75 bp paired-end chemistry (Welcome Trust Centre for Human Genetics).

Raw sequencing reads were trimmed with Cutadapt v2.9 before mapping to the mm10 version of the mouse genome using Bowtie2 v2.3.5 with the following parameters: --local--X 2000. PCR duplicates were removed with Picard Tools v2.22.3; additionally, reads mapping to chrM, with a mapping quality <10 and insert sizes >150 bp were removed before peak calling. Peaks were called with model-based analysis of ChIP–seq (MACS2 v2.2.6) with the following settings: --format BAMPE--nomodel--keep-dup all--mfold 5 50. Peaks found in at least two biological replicates were kept for further analysis and the merged peakset consisting of all discovered peaks was used for differential accessibility testing. Reads were counted over the merged peakset using BedTools v2.29.2 and tested using DESeq2. Significantly DAPs were deemed as having $P_{adj} < 0.05$ (likelihood ratio test), $P_{adj} < 0.05$ and fold change >1.5 (Wald test). Gene ontology was conducted using GREAT v4.0.4 (ref. [55]). DeepTools v3.3.0 was used to generate normalized bigWigs from all biological replicates, which were merged for visualization in the Integrative Genomics Viewer. ATAC-seq peaks were annotated with the nearest gene and comparisons between mRNA and ATAC-seq data were limited to genes with ATAC-seq peaks within 2.5 kb of the transcription start site.

De novo motif discovery was conducted on DNA sequences from the central regions of DAPs. DNA sequences were softmasked to remove repetitive regions and custom background sequences were created from the flanking regions of the DNA sequences with the fasta-get-markov -m 2 command. Motif analysis was then performed using MEME-ChIP v5.3.1 (ref. [56]) with the options: -meme-minw 5 -meme-maxw 30 - meme-nmotifs 10. The motif discovery mode (-meme-mod) option was set to zero or one occurrence per sequence (zoops). To find the occurrences of known motifs within ATAC-seq peaks, FIMO (find individual motif occurrences)[56] was used with 1,000-bp sequences centered on the ATAC-seq peak summits; peak flanking regions of equal lengths were used for the background, as above.

Generation of HoxB8 neutrophils with targeted knockouts. HoxB8 C57BL/6N myeloid progenitors and stem cell factor (SCF)-producing CHO cells were kindly provided by B. Walzog (LMU Biomedizinsches Centrum). HoxB8 myeloid progenitors were tested for *Mycoplasma* and routinely cultured in RMPI 1640 medium supplemented with 10% FCS, 30 mM of β-mercaptoethanol (Thermo Fisher Scientific), 1% supernatant from SCF-producing CHO cells and 1 µM of β-estradiol (Sigma-Aldrich). Differentiation was induced by estrogen removal and culture in medium containing 1% SCF supernatant. Progenitor cells were differentiated into neutrophils by culturing with complete RPMI 1640 medium supplemented with 30 µM of β-mercaptoethanol, 4% SCF containing supernatant and 20 ng ml^{-1} granulocyte colony-stimulating factor in a 5% CO_2 tissue culture incubator at 37 °C. To generate CRISPR–Cas9-mediated knockout, progenitors were transduced with lentiCas9-v2 lentiviruses targeting exon 1 of CEPBb (ENSMUSG00000056501; guide RNA (gRNA) AGGCTCACGTAACCGTAGT), exon1 of KLF6 (ENSMUSG00000000078, gRNA TCGCTGTCGGGAAAACAGGG), exon3 of Runx1 (ENSMUSG00000022952, gRNA TAGCGAGATTCAACGACCTC), exon5 of RFX2 (ENSMUSG00000024206, gRNA CTGCTGGGGGCGTAAAGCTG), exon4 of RELB (ENSMUSG00000002983, gRNA CTGCACGGACGGCGTCTGCA), exon2 of IRF5 (ENSMUSG00000029771, gRNA ACCCTGGCGCCATGCCACGAGG) and exon1 of JUNB (ENSMUSG00000052837, gRNA GGAACCGCAGACCGTACCGG). Briefly, lentiCas9-v2 lentivirus was produced from HEK-293FT cells transfected with the lentiCas9-v2 plasmid mixed with the lentiviral packaging plasmids pVSVG (plasmid no. 8454; Addgene) and psPAX2 (plasmid no. 12260; Addgene). Then, 48 h posttransfection, the lentivirus-containing supernatants were collected, filtered and selected with 6 µg ml^{-1} puromycin for the targeted knockout of C/EBPβ, KLF6, RUNX1, RFX2, RELB, IRF5 and JUNB.

Cytospin. For morphological analysis, differentiated HoxB8 neutrophils were spun onto glass slides by centrifugal forces using a Thermo Shandon Cytospin 3 Cytocentrifuge (Thermo Fisher Scientific) at 400*g* for 5 min. The slides were stained with ready-to-use modified Wright–Giemsa stain from Sigma-Aldrich (catalog no. WG16) according to the manufacturer's protocol. Images were obtained from stained slides under bright field using an Olympus BX51 fluorescence microscope (Olympus).

Western blots. Cells were lysed in 1% Triton X-100 lysis buffer (1% v/v Triton X-100, 10% v/v glycerol, 1 mM of EDTA, 150 mM of NaCl, 50 mM of Tris, pH 7.8) supplemented with protease inhibitor cocktails (Roche). Lysates were incubated on ice for 30 min and cleared by centrifugation at 13,000 r.p.m. for 10 min at 4 °C. Protein quantification was performed with the Qubit assay (Thermo Fisher Scientific) according to the manufacturer's protocol; 20 µg of lysates were boiled in Laemmli sample buffer (Bio-Rad Laboratories), resolved on a NuPAGE 4–12% Bis-Tris gel (Invitrogen) and transferred onto a polyvinylidene difluoride membrane (GE Healthcare) by wet western blot. Membranes were blotted for primary antibodies (Supplementary Table 1), followed by IRDye-conjugated secondary antibodies. Complexes were detected with the Odyssey Infrared Imaging System (LI-COR) and analyzed using Image Studio Lite v.5.2.5 (LI-COR).

Estimation of mitochondrial transmembrane potential. Mitochondrial transmembrane potential was monitored with the voltage-sensitive fluorescence indicator tetramethylrhodamine, methyl ester (TMRM). For that, HoxB8 neutrophils (2 × 10^6 cells ml^{-1}) were loaded with 200 nM of TMRM for 20 min. TMRM fluorescence was estimated using a BD LSR II flow cytometer.

Metabolic flux analysis. The real-time extracellular acidification rate and OCR were measured using a XF96 extracellular flux analyzer (Seahorse Bioscience); 2×10^6 HoxB8 neutrophils were washed twice in RPMI 1640 without sodium bicarbonate, 20 mM of glucose, 1% FCS and 2 mM of pyruvate and seeded in corresponding assay medium in an XF plate coated with poly-L-lysine (Sigma-Aldrich). Neutrophils were rested at 37 °C for 1 h before analysis. Three independent experiments were performed with four independent replicates per group.

Intracellular ROS measurement. Intracellular ROS were measured using a FACS-based method. HoxB8 neutrophils were incubated with 2.5 μg ml^{-1} (7 μM) dihydrorhodamine 123 (Thermo Fisher Scientific) in complete RPMI 1640 medium and stimulated with 50 nM of phorbol 12-myristate 13-actetate (PMA) (Sigma-Aldrich) for 20 min at 37 °C. Cells were subsequently washed with PBS and the fluorescence intensity of each subset/cells was measured by flow cytometry.

Phagocytosis. The phagocytosis capacity of HoxB8 neutrophils was measured by FACS-based method using fluorescent *E. coli* (product no. 25922GFP; ATCC). Briefly, HoxB8 neutrophils were incubated with fluorescent *E. coli* at a multiplicity of infection of 10 in complete RPMI 1640 medium for 15 min at 37 °C. Neutrophils were subsequently washed with PBS and the fluorescence intensity of each subset/cells was measured by flow cytometry.

Bacterial killing assay. The bacterial killing assay was performed with *S. aureus* (NCTC no. 6571), which was used at a multiplicity of infection of 10. For the bacterial killing assay, HoxB8 neutrophils were infected for 2 h with *S. aureus* and then lysed in 1% Triton X-100 buffer; the lysate was plated on agar plates. Bacterial culture plates were incubated at 37 °C overnight and the colony number on each plate was counted the following morning as an absolute colony-forming unit (CFU) count.

NETosis. To induce NETosis, HoxB8 neutrophils were seeded into an 8-well Nunc Lab-Tek II Chamber Slide (VWR international) coated with 2% poly-lysine (Sigma-Aldrich) at a volume of 100 μl at the density of 1×10^6 ml^{-1}. Neutrophils were stimulated with 5 μM of ionomycin and PMA (Sigma-Aldrich) overnight at 37 °C in a 5% CO_2 tissue culture incubator and were subsequently fixed with 4% paraformaldehyde (Sigma-Aldrich) in Dulbecco's PBS for 30 min at room temperature. After blocking, the primary antibodies rabbit anti-citrullinated histone 4 (catalog no. ab5103; Abcam) and mouse anti-mouse MPO (catalog no. HM1051BT; Hycult) were added at a 1:100 dilution overnight at 4 °C. Cells were washed with Dulbecco's PBS before adding secondary antibodies: mouse anti-rabbit DyLight 647-conjugated secondary antibody (Thermo Fisher Scientific) and rabbit anti-mouse IgG secondary antibody conjugated with Alexa Fluor 488 (Thermo Fisher Scientific). Images were obtained using an Olympus BX51 fluorescence microscope. Neutrophils with a clear formation of fibers stained by citrullinated histone 3, colocalized with a diffuse nucleus stained by SYTOX and colocalization with MPO, were counted as neutrophils under NETosis. Images were analyzed using Fiji v.2.1.0/1.53h.

Cell viability. A total of 10,000 cells per well HoxB8 myeloid progenitors were seeded and differentiated for 5 d. Cell viability was assessed using annexin V staining and Fixable Viability Dye eFluor 780 LIVE/DEAD staining (Thermo Fisher Scientific) and analyzed by flow cytometry to determine the percentage undergoing apoptosis. Samples were tested in triplicate and normalized to fluorescence minus one (FMO) wells.

Neutrophil migration assay with Boyden chamber. For the neutrophil migration assay, Hoxb8 neutrophils were washed with the migration medium RPMI 1640 containing 2.5 mM of HEPES and 0.1% BSA and tested for migration in a 96-well microchamber using a 5-μm pore size polycarbonate filter (Neuro Probe). The lower wells of the Boyden chamber were filled with the migration medium supplemented with either PBS or 10 nM of murine recombinant chemokine (C-C motif) ligand 3 (Ccl3) (R&D). In the upper wells, 5×10^4 Hoxb8 neutrophils were added and the chamber was incubated for 90 min at 37 °C and 5% CO_2. After incubation, nonmigrating cells in the upper chamber were removed using a cotton-tipped applicator. Cells that had migrated to the bottom of the membrane were fixed in 70% ethanol and stained with 4,6-diamidino-2-phenylindole before mounting onto poly-L-lysine-coated slides. Each condition was performed in duplicate. The number of migrated neutrophils counted in five random fields was analyzed using Fiji.

RNA extraction and quantitative PCR with reverse transcription. Total RNAs were isolated from cells using the RNeasy Mini Kit and reverse-transcribed to cDNA using the High-Capacity cDNA Reverse Transcription Kit (Thermo Fisher Scientific) according to the manufacturer's protocol. RNA from sorted cells was isolated utilizing the RNeasy Micro Kit (QIAGEN). Real-time PCR reactions were performed on a ViiA7 system (Thermo Fisher Scientific) with TaqMan primer sets (Supplementary Table 1). Gene expression was analyzed using the comparative Ct ($\Delta\Delta^{Ct}$) method and normalized against the levels of the housekeeping gene *Hprt* as the arbitrary unit.

Measurement of cytokine production. For the cytokine array, 1×10^6 HoxB8 neutrophils seeded in 2 ml of RPMI 1640 were stimulated with 50 μg ml^{-1} zymosan or DMSO vehicle for 2 h. The Mouse Cytokine Array, Panel A (catalog no. ARY006; R&D Systems) was used to simultaneously detect the levels of 40 different cytokines and chemokines in 400 μl of supernatant of stimulated HoxB8 neutrophils, according to the manufacturer's instructions. Signals were detected by chemical luminescence and subsequently quantitated with Image Studio.

Adoptive transfer of HoxB8 neutrophils. HoxB8 neutrophils were transferred intravenously into mice subjected to the air pouch model of in vivo inflammation, as shown in Supplementary Fig. 2. WT and knockout HoxB8 neutrophils were labeled with CellTrace Far Red (Thermo Fisher Scientific) and CellTrace CFSE (Thermo Fisher Scientific), respectively, at a final concentration of 5 μM according to the manufacturer's procedure. Next, 10×10^6 differentially labeled WT and knockout neutrophils were mixed at an equal ratio and adoptively transferred into the air pouch model of in vivo inflammation at a volume of 300 μl, followed by subcutaneous zymosan stimulation. Four hours postzymosan challenge, blood, membrane and exudate were collected for flow cytometry.

Model of AMI. Female 8–12-week-old mice were subjected to 45 min occlusion of the left anterior descending (LAD) coronary artery followed by 1 h reperfusion (for infarct size), as described previously[6]. Briefly, fully anesthetized animals were intubated and temperature-controlled throughout the experiment at 36.5 °C to prevent hypothermic cardioprotection. Thoracotomy was then performed and the LAD was ligated with a nylon 8/0 monofilament suture for 45 min. To quantify infarct size, mice were re-anesthetized and reintubated and the LAD coronary artery was reoccluded by ligating the suture in the same position as the original infarction. Animals were then humanely killed and 1 ml of 1% Evans Blue dye (Sigma-Aldrich) was infused intravenously to delineate the AAR (myocardium lacking blood flow, that is, negative for blue dye staining). The left ventricle was isolated, cut into transverse slices (5–7 1-mm thick slices per left ventricle) and both sides were imaged. To delineate the infarcted (necrotic) myocardium, slices were incubated in TTC (Sigma-Aldrich) at 37 °C for 15 min. The slices were then rephotographed, weighed and regions negative for Evans Blue staining (AARs) and for TTC (infarcted myocardium) were quantified using ImageJ v2.1.0/1.53h (NIH). The percentage values for AARs and infarcted myocardium were corrected to mg independently for each slice. Absolute AAR and infarct size were determined as the mg:mg ratio of AAR:left ventricle and infarcted myocardium:AAR, respectively.

Mixed bone marrow chimera and AMI. Recipient WT C57BL/6 mice were lethally irradiated (two 6-Gy doses, 3 h apart) before receiving 1 million bone marrow nucleated cells by intravenous injection. For mixed chimeras, equal numbers of donor CD45.1 or *S100a8*^{Cre} *Junb*$^{loxP/loxP}$ bone marrow cells, collected by flushing the femur with PBS, were mixed before intravenous injection. Engraftment of recipient animals was assessed six weeks after transplantation by analysis of the percentage of CD45.1 or CD45.2 leukocytes in the blood by flow cytometry. Eight weeks after transplantation, mice were subjected to 45 min occlusion of the LAD coronary artery followed by 3 h reperfusion. Heart, blood and bone marrow were collected and processed for flow cytometry analysis. Briefly, blood was taken through cardiac puncture, the bone marrow cells of mice were flushed from femurs using a 23-G needle and hearts were collected and cut dry into small pieces before being digested in liberase TM (Roche) and DNase1 (Sigma-Aldrich) for 45 min at 37 °C and homogenized into single-cell suspensions using 70-mm nylon mesh sieves and syringe plungers. Single-cell suspensions were lysed in red blood cell lysis buffer (eBioscience) for 4 min, stained with fluorochrome-conjugated antibodies and then fixed and permeabilized using the Fix & Perm and Perm buffers (eBiosciences) according to the manufacturer's instructions to determine pro-IL-1B production or incubated with 2.5 μg ml^{-1} of dihydrorhodamine 123 (Invitrogen) at 37 °C for 20 min to quantify ROS.

Statistical analysis. Prism 8.0 (GraphPad Software) was used for data analysis. Data are represented as the mean ± s.d. Unless otherwise noted, statistical significance was determined by unpaired, two-tailed Student's *t*-test for two-group comparisons, one-way analysis of variance (ANOVA) with Dunnett's multiple comparisons test for comparisons of more than two groups and two-way ANOVA for comparisons of more than two groups with two or more time points. $P<0.05$ was considered statistically significant, where $^*P<0.05$, $^{**}P<0.01$, $^{***}P<0.001$ and $^{****}P<0.0001$.

Reporting Summary. Further information on research design is available in the Nature Research Reporting Summary linked to this article.

Data availability

The RNA-seq (Fig. 1) and ATAC-seq (Fig. 2) data that used neutrophils from mice subjected to air pouch and zymosan stimulation and the RNA-seq data using the HoxB8 neutrophils (Figs. 5 and 7 and Extended Data Figs. 7–9) are available at the Gene Expression Omnibus (GEO) under accession no. GSE161765. The previously published RNA-seq data with accession nos. GSE147910 and GSE109125 were retrieved from the GEO. To align the neutrophil subpopulations from the

bone marrow, blood, air pouch membrane and exudate in the current study (Extended Data Fig. 1i), we also utilized published scRNA-seq data (accession no. GSE137540). Source data are provided with this paper.

Code availability

All code used in current study has been stored at https://github.com/Tariq-K?tab=repositories.

References

53. Love, M. I., Huber, W. & Anders, S. Moderated estimation of fold change and dispersion for RNA-seq data with DESeq2. *Genome Biol.* **15**, 550 (2014).
54. Buenrostro, J. D., Giresi, P. G., Zaba, L. C., Chang, H. Y. & Greenleaf, W. J. Transposition of native chromatin for fast and sensitive epigenomic profiling of open chromatin, DNA-binding proteins and nucleosome position. *Nat. Methods* **10**, 1213–1218 (2013).
55. McLean, C. Y. et al. GREAT improves functional interpretation of *cis*-regulatory regions. *Nat. Biotechnol.* **28**, 495–501 (2010).
56. Machanick, P. & Bailey, T. L. MEME-ChIP: motif analysis of large DNA datasets. *Bioinformatics* **27**, 1696–1697 (2011).

Acknowledgements

We are grateful to Jonathan Webber (Kennedy Institute of Rheumatology (KIR), Nuffield Department of Orthopaedics, Rheumatology and Musculoskeletal Sciences (NDORMS)) for providing the cell sorting service, T. Nicol and M. Crabtree (Nuffield Department of Medicine) for help with the Seahorse assay the and Genomic core facility (Wellcome Centre for Human Genetics) for sample sequencing and technical support. We thank F. Powrie for scientific discussions and E. Thompson and D. Berthold (KIR, NDORMS) for helpful suggestions on the manuscript and assistance with figures. This work was supported by the Oxford-Celgene fellowship (T.E.K.); the Chinese Science Council (Z.A.); Wellcome Trust Investigator Award no. 209422/Z/17/Z to I.A.U., E.v.G. and H.E.; Novo Nordisk Foundation Tripartite Immunometabolism Consortium (no. NNF15CC0018486 to S.M. and L.W.); and the Erasmus Foundation (N.W. and V.v.W.).

Author contributions

I.A.U. conceptualized the study. I.A.U., S.M., H.E., T.E.K. and Z.A. devised the methodology. T.E.K., Z.A., S.M., H.E., I.B., S.M-S., L.W., N.W., V.v.W. and A. Hemmings carried out the experiments. T.E.K., Z.A., I.B., E.v.G. and I.A.U. analyzed and/or interpreted the experimental data. T.E.K. and Z.A. carried out the computational genomic analysis. A.Z. and B.W. provided the materials. I.A.U., Z.A., A. Hidalgo, T.E.K., E.v.G. and H.E. wrote, reviewed and edited the manuscript.

Competing interests

The authors declare no competing interests.

Additional information

Extended data is available for this paper at https://doi.org/10.1038/s41590-021-00968-4.

Supplementary information The online version contains supplementary material available at https://doi.org/10.1038/s41590-021-00968-4.

Correspondence and requests for materials should be addressed to I.A.U.

Peer review information *Nature Immunology* thanks the anonymous reviewers for their contribution to the peer review of this work. Z. Fehervari was the primary editor on this article and managed its editorial process and peer review in collaboration with the rest of the editorial team. Peer reviewer reports are available.

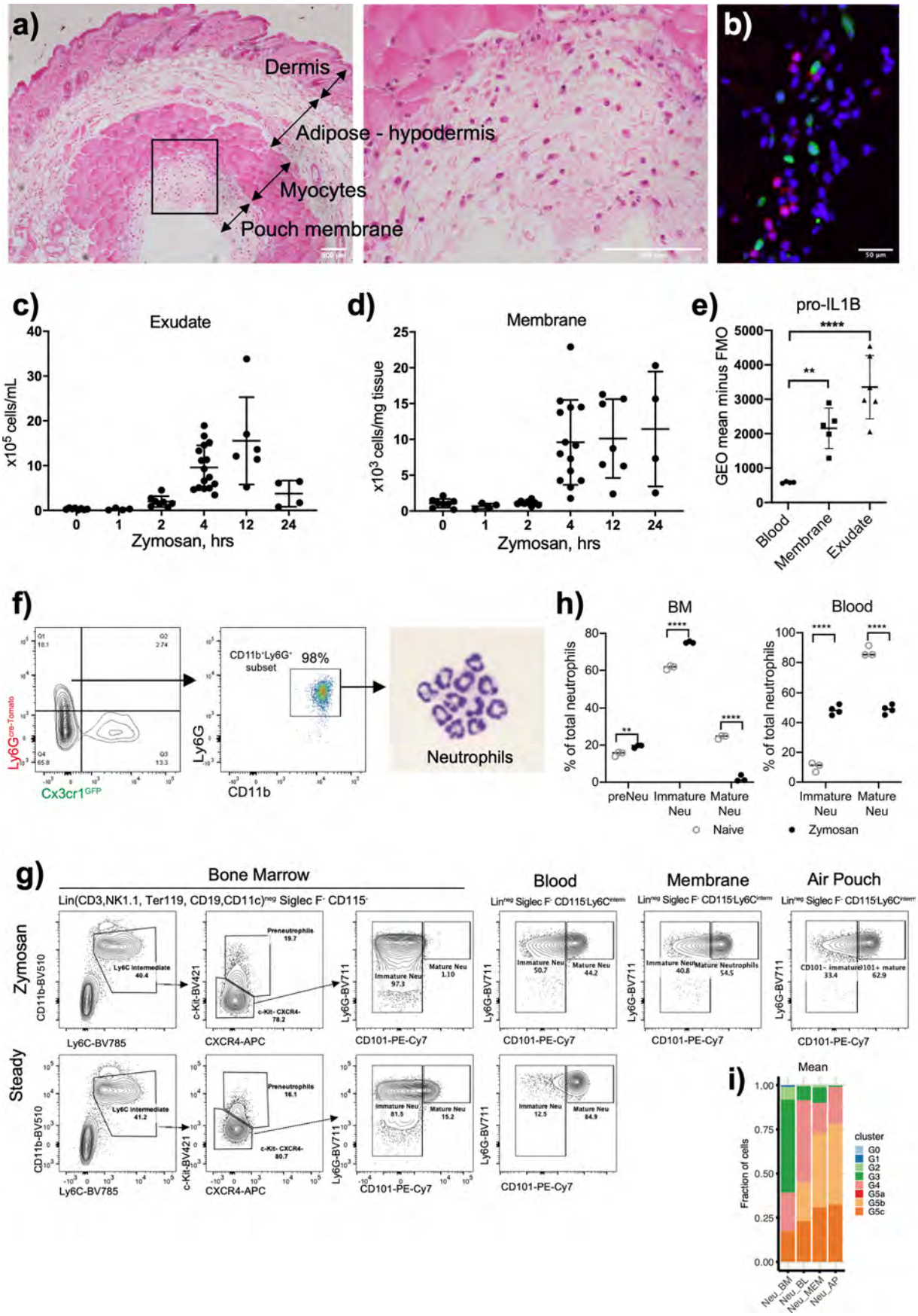

Extended Data Fig. 1 | See next page for caption.

Extended Data Fig. 1 | Administration of zymosan into the air pouch cavity induces neutrophil transcriptional remodeling. a, Representative H&E staining showing the formation of the granulation tissue (membrane) and infiltration of leukocytes. Representative (left) and zoomed-in (right) images of air pouch cavity from mice subjected to air pouch and zymosan challenge are shown with indicated scale bars. **b**, Representative image of immunofluorescence imaging on the pouch cavity of *Ly6g*$^{cre\text{-}tdTomato}$ *x Cx3cr1*^{GFP} illustrates typical neutrophil infiltration. Neutrophils and macrophages appear reddish and green, respectively, and cell nuclei stained with DAPI appear blue. a, b) Representative images from four mice are shown. **c**, Total number of neutrophils per milliliter of air-pouch exudate (AP) post challenge with zymosan. **d**, Total number of neutrophils per milligram of air-pouch membrane (MEM) post challenge with zymosan. **e**, Expression of pro-IL1β, as measured by flow cytometry, in neutrophils from indicated tissues recovered from mice subjected to the air pouch model and zymosan challenge. c, d, e) Results are the means and SD of 15 mice. Significant differences are denoted as: *P < 0.05, **P < 0.01, ***P < 0.001, and ****P < 0.0001; (DM one-way ANOVA with Dunnett's multiple comparisons test). **f**, Gating strategy of neutrophil sorting from *Ly6g*$^{cre\text{-}tdTomato}$ *x Cx3cr1*^{GFP} mice for subsequent RNA sequencing analysis and ATAC sequencing analysis. **g**, Gating strategy used to quantify neutrophils under different maturation stages. **h**, Percentage distribution of neutrophil subsets in BM and blood between steady condition and zymosan-induced inflammation. Data are shown as means and SD from three naïve mice and four mice with zymosan challenge. Significant differences are denoted as: **P < 0.01, ****P < 0.0001 (RM two-way ANOVA with Šidák's multiple comparisons test). **i**, Correlation between indicated neutrophil samples with scRNA-seq-defined neutrophil populations reported by Xie et al.[11]. The mean fraction of indicated scRNA-seq defined clusters (G0-G5) in each group of neutrophil samples. G0-G4: BM neutrophils (G0-CMP, G1-GMP, G2-pre-neutrophils; G3-immature neutrophils; G4-mature neutrophils). G5a, G5b, G5c: peripheral mature neutrophils.

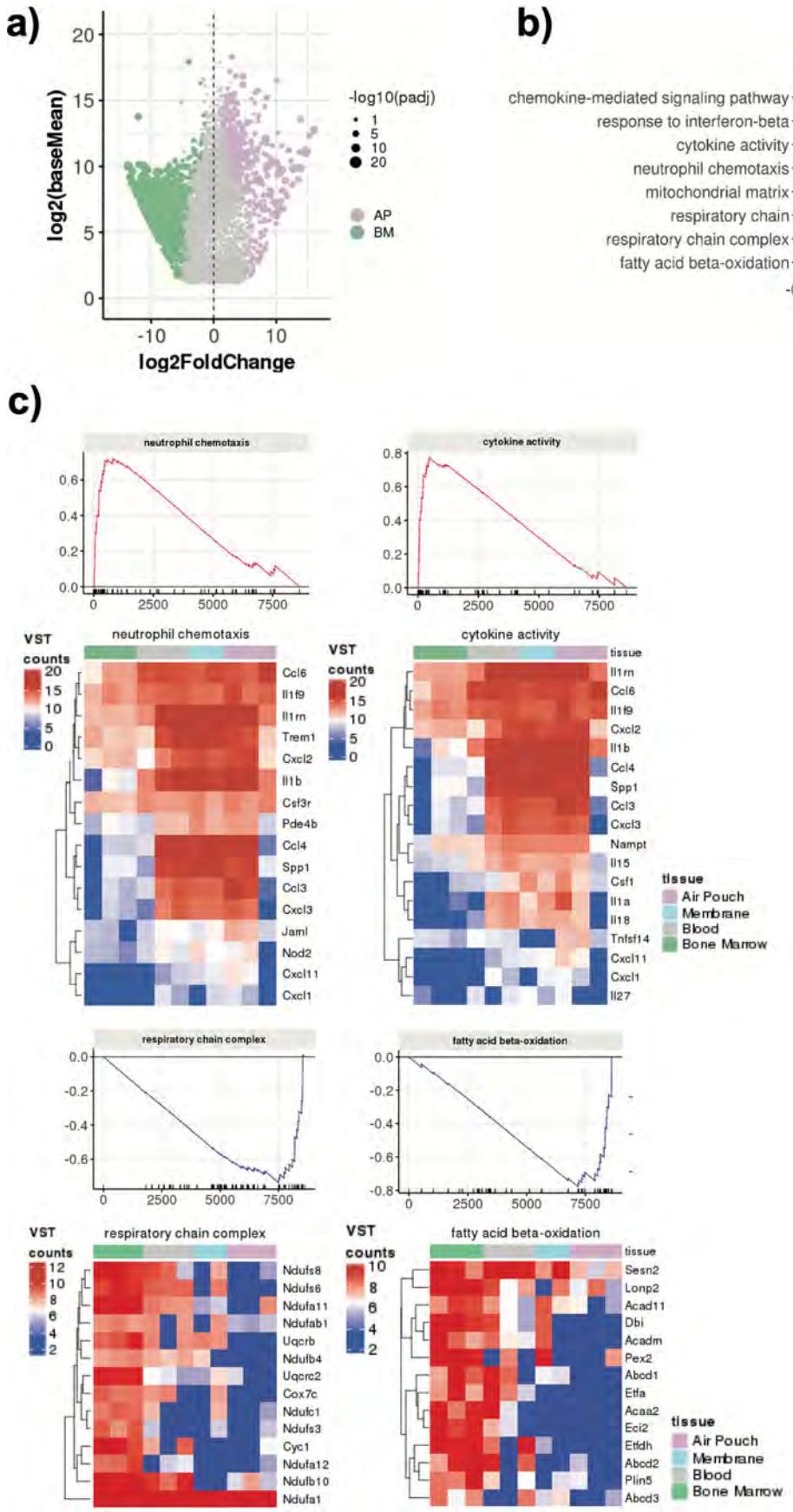

Extended Data Fig. 2 | See next page for caption.

Extended Data Fig. 2 | Analysis of DEG expression reveals gene set enriched pathways. a, Global changes in gene expression between the bone marrow and air pouch (padj < 0.05, fold change > 1.5). **b**, Top gene ontology terms associated with the bone marrow and air pouch identified by gene set enrichment analysis (GSEA) padj < 0.01. **c**, Gene set enrichment analysis (GSEA) of genes differentially expressed between the bone marrow and air pouch. Line plot shows the distribution of genes ranked by their normalised enrichment score (ES). Heatmaps show variance stabilised counts of the leading-edge genes most associated with each tissue.

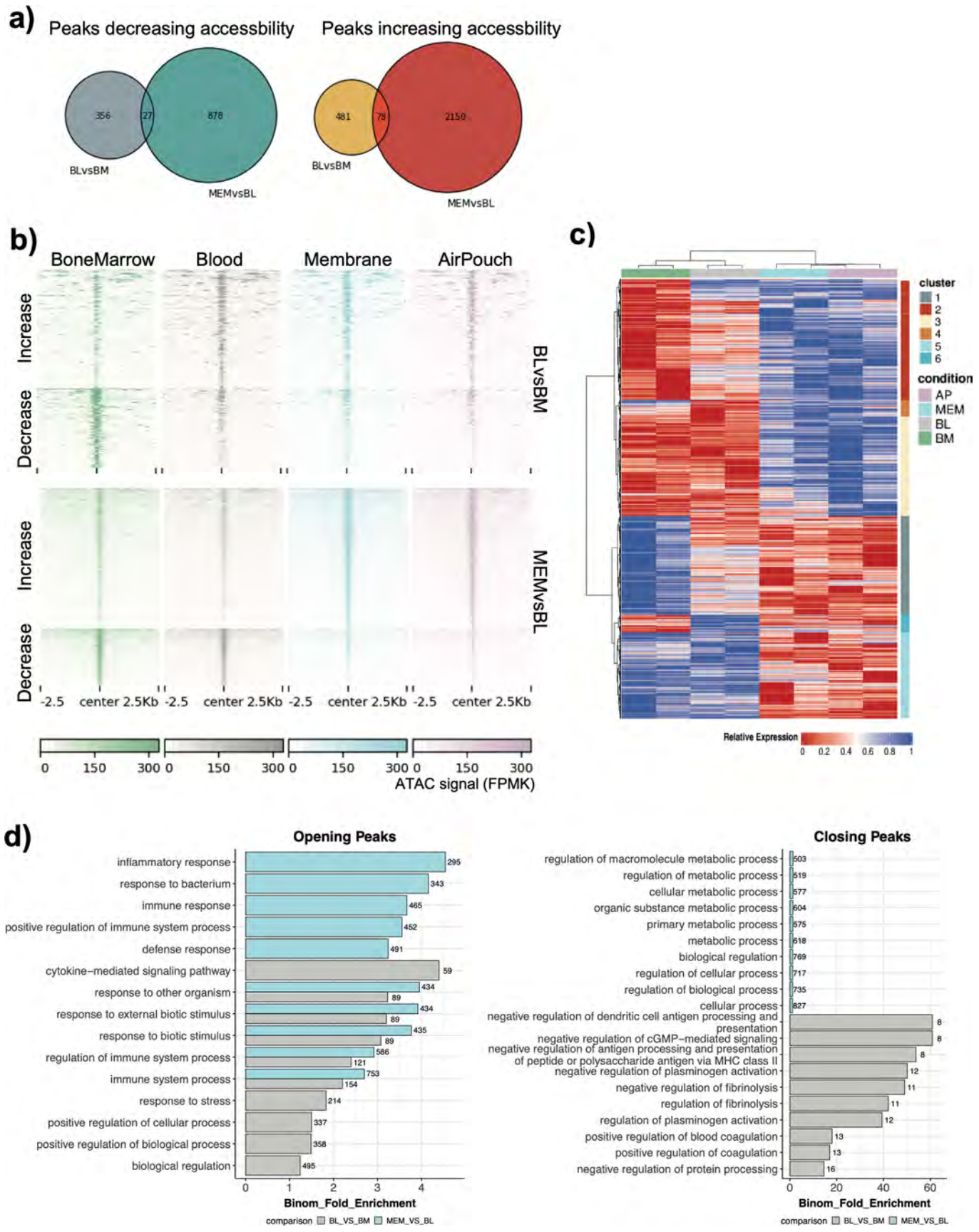

Extended Data Fig. 3 | See next page for caption.

Extended Data Fig. 3 | Discrete changes occur in neutrophil chromatin landscape *en route* to the site of inflammation. a, Venn diagrams showing the overlap of differentially accessible peaks (padj < 0.05, fold change > 1.5) between the indicated transitions. **b**, Heat maps of normalised read counts (FPKM) over 2.5 k.b regions centred on ATAC-seq peaks from each tissue. Only differentially accessible peaks between the blood and bone marrow, and between blood and membrane are shown (padj < 0.05, fold change > 1.5). **c**, Hierarchical clustering of all differentially accessible peaks (LRT test padj < 0.01) based on Manhattan distances using the Ward method. Data are presented as a heatmap normalised to the minimum and maximum of each row. **d**, Gene ontology analysis for differentially accessible peaks between the blood and bone marrow, and between blood and membrane (padj < 0.05, fold change > 1.5). The top 10 most significant results are shown and the number of differentially accessible peaks within each GO term are annotated.

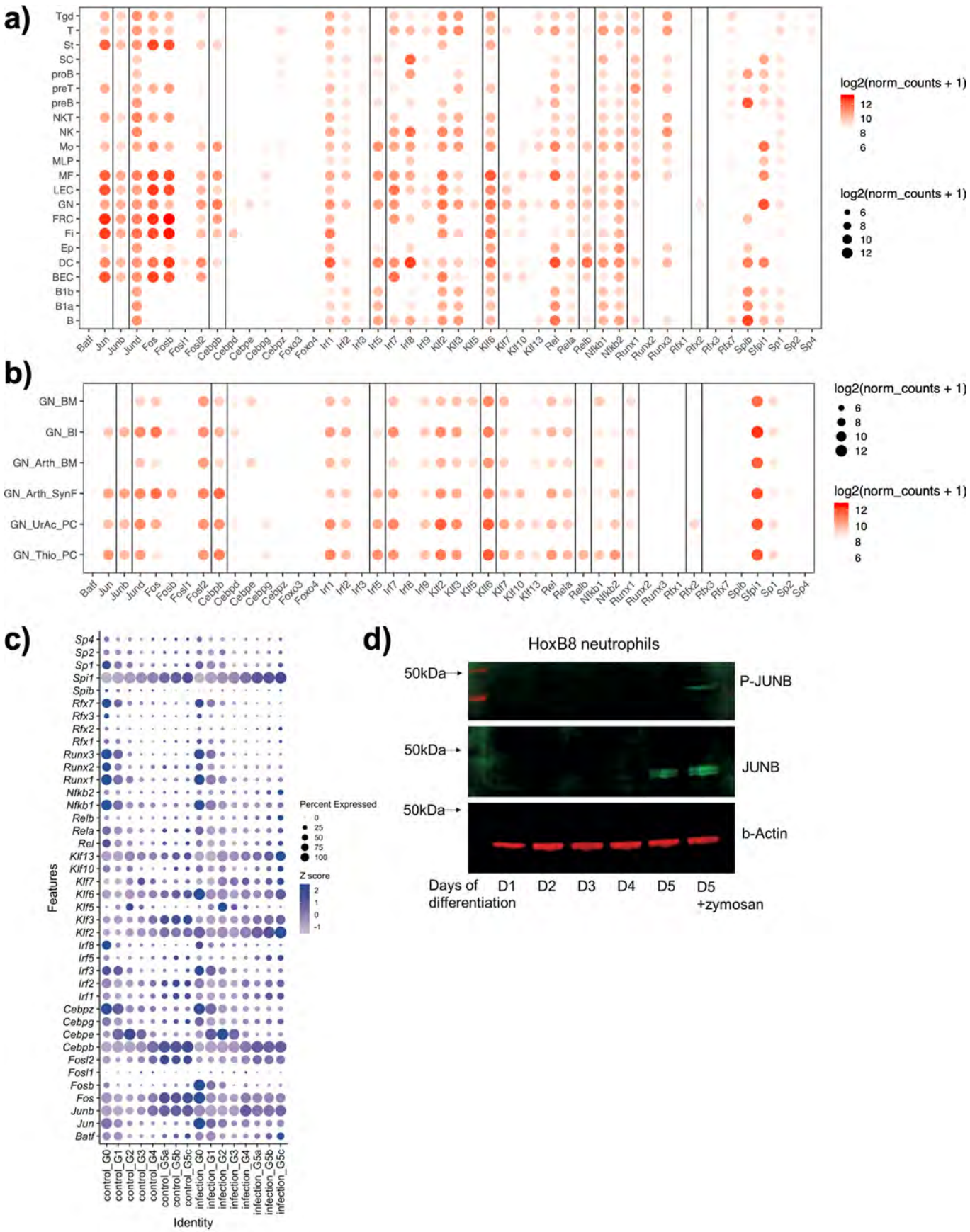

Extended Data Fig. 4 | See next page for caption.

Extended Data Fig. 4 | Expression of predicted transcription factor family members in neutrophils. a, Expression of identified transcription factor (TF) family members across immune cell populations (ImmGen), subpopulation level counts are averaged. Highlighted TFs have high levels of neutrophil expression. **b**, Expression of predicted transcription factor (TF) family members across neutrophil sub-populations (ImmGen). Highlighted TFs have high levels of neutrophil expression and/or neutrophil specific expression compared with other family members. **c**, Expression of predicted transcription factors in each of G0 to G5 clusters, mapped to progressively maturing neutrophils in scRNA-Seq analysis[11], before and after intraperitoneal *E. coli* challenge, coloured by the average expression of each gene in each cluster scaled across all clusters. **d**, Western blot analysis of JUNB activation (P-JUNB) and levels of expression (JUNB) over the time course of HoxB8 neutrophil differentiation/maturation (D0 to D5) and under zymosan stimulation, and representative blot from three independent experiments is shown.

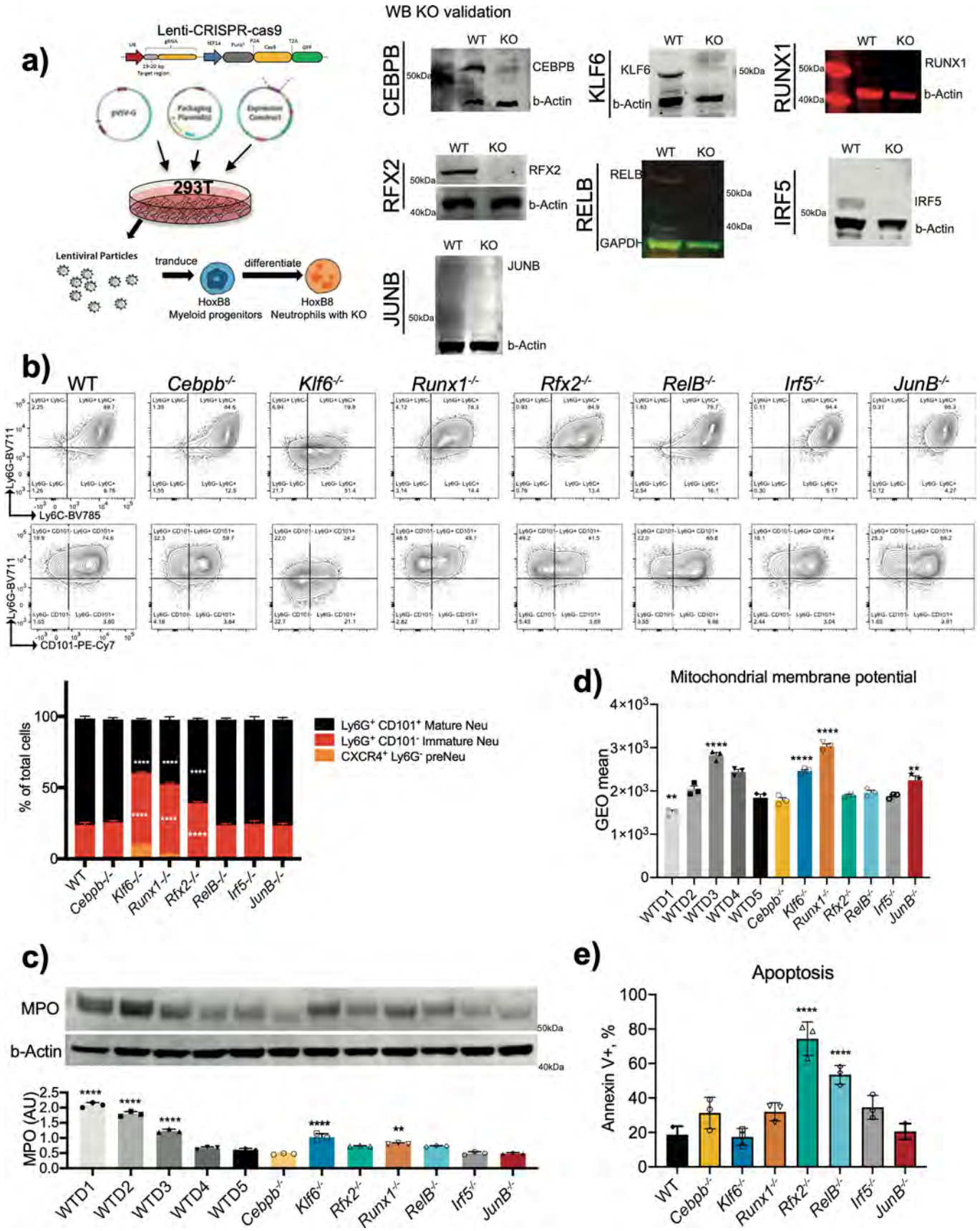

Extended Data Fig. 5 | See next page for caption.

Extended Data Fig. 5 | Validation and maturation of TF knockout neutrophils. a, Targeted TF knockout of HoxB8 neutrophils. Left: Schematic of *in vitro* generation, CRISPR-Cas9 lentivirus transduction and subsequent differentiation into neutrophils in the presence of G-CSF. Right: Immunoblots for validating TF knockout from HoxB8 neutrophils, and representative blots from three independent experiments are shown. **b**, Representative flow cytometry plots(top) of WT or *CEBPβ*$^{-/-}$, *Klf6*$^{-/-}$, *Runx1*$^{-/-}$, *Rfx2*$^{-/-}$, *RelB*$^{-/-}$, *Irf5*$^{-/-}$ or *JunB*$^{-/-}$ HoxB8 neutrophils co-labelled with Ly6C, Ly6G and CD101. Quantification of flow cytometry data as percentages of preneutrophils Ly6G^{-}CXCR4^{+}, immature Ly6G^{+}CD101^{-} and mature Ly6G^{+}CD101^{+} neutrophils (bottom). Data are shown as means and SD and are representative of three independent experiments. Significant differences compared with the WT control group are denoted as: ****$P < 0.0001$ (two-way ANOVA with Dunnett's multiple comparisons test). **c**, Myeloperoxidase (MPO) expression in HoxB8 neutrophils. A representative Western blot probed with antibodies specific for MPO and b-Actin is shown. MPO expression is normalized against b-Actin amount in the lysates (and expressed as arbitrary unit of MPO). **d**, Mitochondrial transmembrane potential of WT and indicated KO HoxB8 neutrophils measured by flow cytometry using TMRM. **e**, Early apoptosis rates of HoxB8 neutrophils differentiated for five days as assessed by the percentage of cells positive for the Annexin V staining and negative for the live/dead staining. Data are shown as means and SD from three independent experiments, each with duplicate. (c, d, e) Data are shown as means and SD and are representative of three independent experiments. Significant differences compared with WT neutrophils are denoted as: **$P < 0.01$, ***$P < 0.001$, ****$P < 0.0001$; (Oridinary one-way ANOVA with Dunnett's multiple comparisons test).

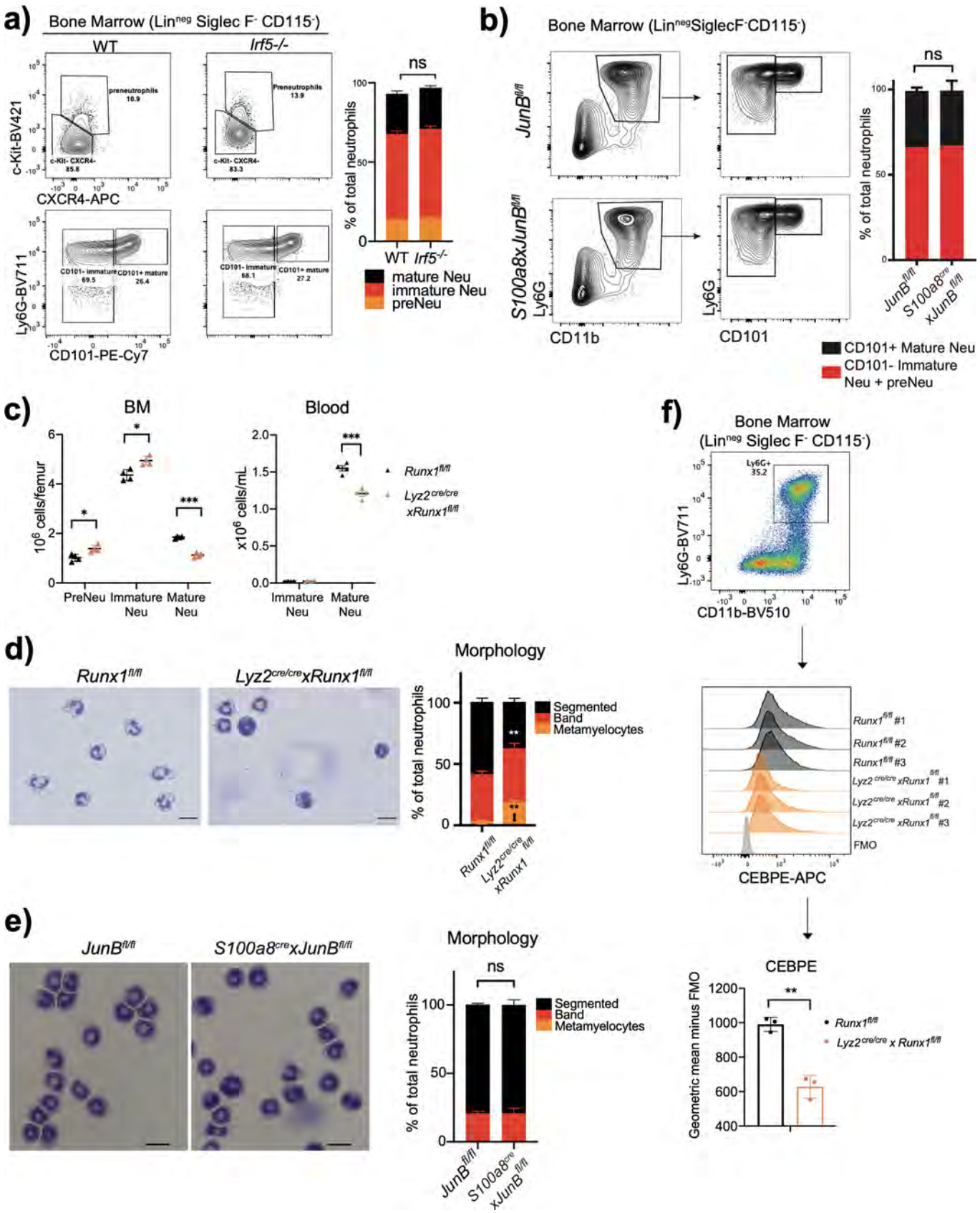

Extended Data Fig. 6 | See next page for caption.

Extended Data Fig. 6 | RUNX1 deficiency impairs neutrophil maturation. a, Irf5 deficiency does not affect neutrophil maturation. Left: representative flow cytometry of neutrophil subsets (pre-neutrophils, immature and mature neutrophils) from WT and *Irf5*$^{-/-}$ mice. **b**, JunB deficiency does not affect neutrophil maturation. Left: representative flow cytometry of neutrophil subsets (pre-neutrophils, immature and mature neutrophils) from *JunB*$^{fl/fl}$ and *S100a8*$^{cre/cre}$*xJunB*$^{fl/fl}$ mice. Right: Statistical analysis of percentages of indicated neutrophil subsets. Data are shown as means and SD derived from three mice from each group. Statistical comparison was made by ordinary one-way ANOVA with Dunnett's multiple comparisons test: ns, no significant difference. **c**, Absolute quantification of neutrophil subsets (pre-neutrophils, immature and mature neutrophils) in the bone marrow (left) and the blood (right) from *Runx1*$^{fl/fl}$ and *Lyz2*$^{Cre/cre}$ *xRunx1*$^{fl/fl}$ mice. **d**, Morphology assessment of CD11b^{+}Ly6G^{+} neutrophils sorted from *Runx1*$^{fl/fl}$ and *Lyz2*$^{Cre/cre}$*xRunx1*$^{fl/fl}$ mice. **e**, Morphology assessment of CD11b + Ly6G+ neutrophils sorted from *JunB*$^{fl/fl}$ and *S100a8*$^{cre/cre}$*xJunB*$^{fl/fl}$ mice. (d, e) Results are expressed as percentages of segmented, banded neutrophils and metamyelocyte out of at least 200 cells counted from different fields and independent replicates. Scale bars represent 10 μm. a, c, d, e) Data are shown as means and SD from three mice from each group within one experiment. Significant differences compared between two individual groups are denoted as: *$P < 0.05$, **$P < 0.01$, ***$P < 0.001$, and ****$P < 0.0001$ (RM two-way ANOVA with Šidák's multiple comparisons test). **f**, Differential expression of Cebpe in CD11b^{+}Ly6G^{+} neutrophils sorted from *Runx1*$^{fl/fl}$ and *Lyz2*$^{Cre/cre}$*xRunx1*$^{fl/fl}$ mice, measured by flow cytometry. Gating strategy (top) of neutrophils for identifying CD11b^{+}Ly6G^{+} neutrophils. Fluorescence histogram (middle) and geometric mean (bottom) of CEBPE expression in CD11b^{+}Ly6G^{+} neutrophils. Data are shown as means and SD derived from three mice from each group. Significant differences compared with *Runx1*$^{fl/fl}$ and *Lyz2*$^{Cer/cre}$*xRunx1*$^{fl/fl}$ mice are denoted as: **$P < 0.01$ (unpaired student t test).

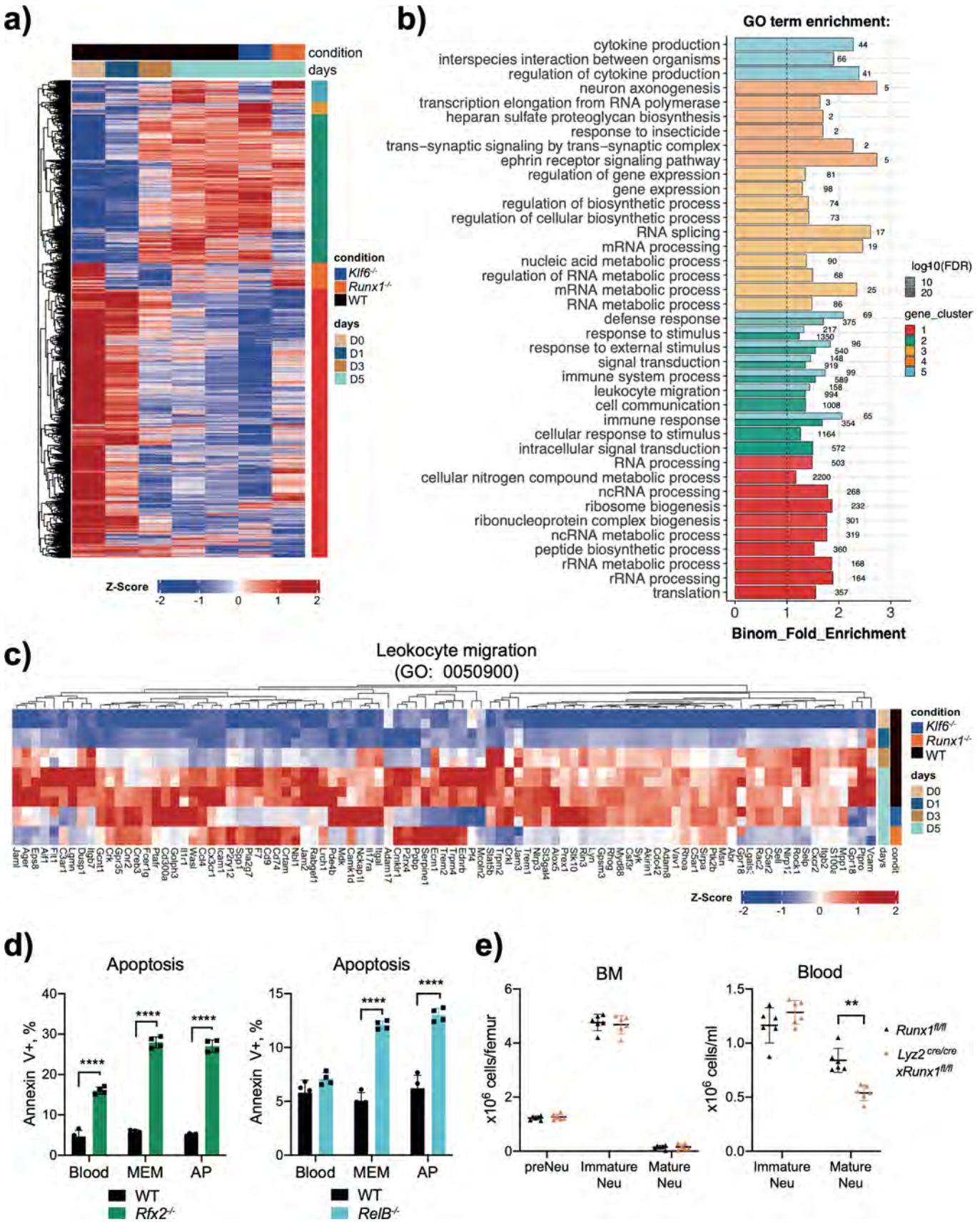

Extended Data Fig. 7 | See next page for caption.

Extended Data Fig. 7 | RUNX1 and KLF6 in transcriptional control of neutrophil migration. a, Hierarchical clustering of all differentially expressed genes (LRT test padj < 0.01, |log2FC|>1), based on Manhattan distances using the Ward method. Data are presented as heatmap normalised to the minimum and maximum of each row. **b**, Gene ontology (GO) analysis, showing the top 10 enriched GO categories for each cluster from Extended Data Fig. 7a. **c**, Leukocyte-migration-related gene expression in WT, *Klf6*$^{-/-}$, or *Runx1*$^{-/-}$ HoxB8 neutrophils. (b, c) Significant differences compared with *Runx1*$^{fl/fl}$ and *Lyz2*$^{Cre/cre}$*xRunx1*$^{fl/fl}$ mice are denoted as: **P < 0.01, ****P < 0.0001 (RM two-way ANOVA with Šidák's multiple comparisons test). **d**, Early apoptosis rates of HoxB8 neutrophils recovered from blood, air pouch membrane and exudate from mice subjected to into air pouch model of acute inflammation and zymosan stimulation, assessed by the percentage of cells positive for the Annexin V staining and negative for the live/dead staining. Data are shown as means and SD from four mice from each group. **e**, Percentage distribution of neutrophil subsets (pre-neutrophils, immature and mature neutrophils) in BM and blood under zymosan-induced inflammation. Data are shown as means and SD from six mice from each group.

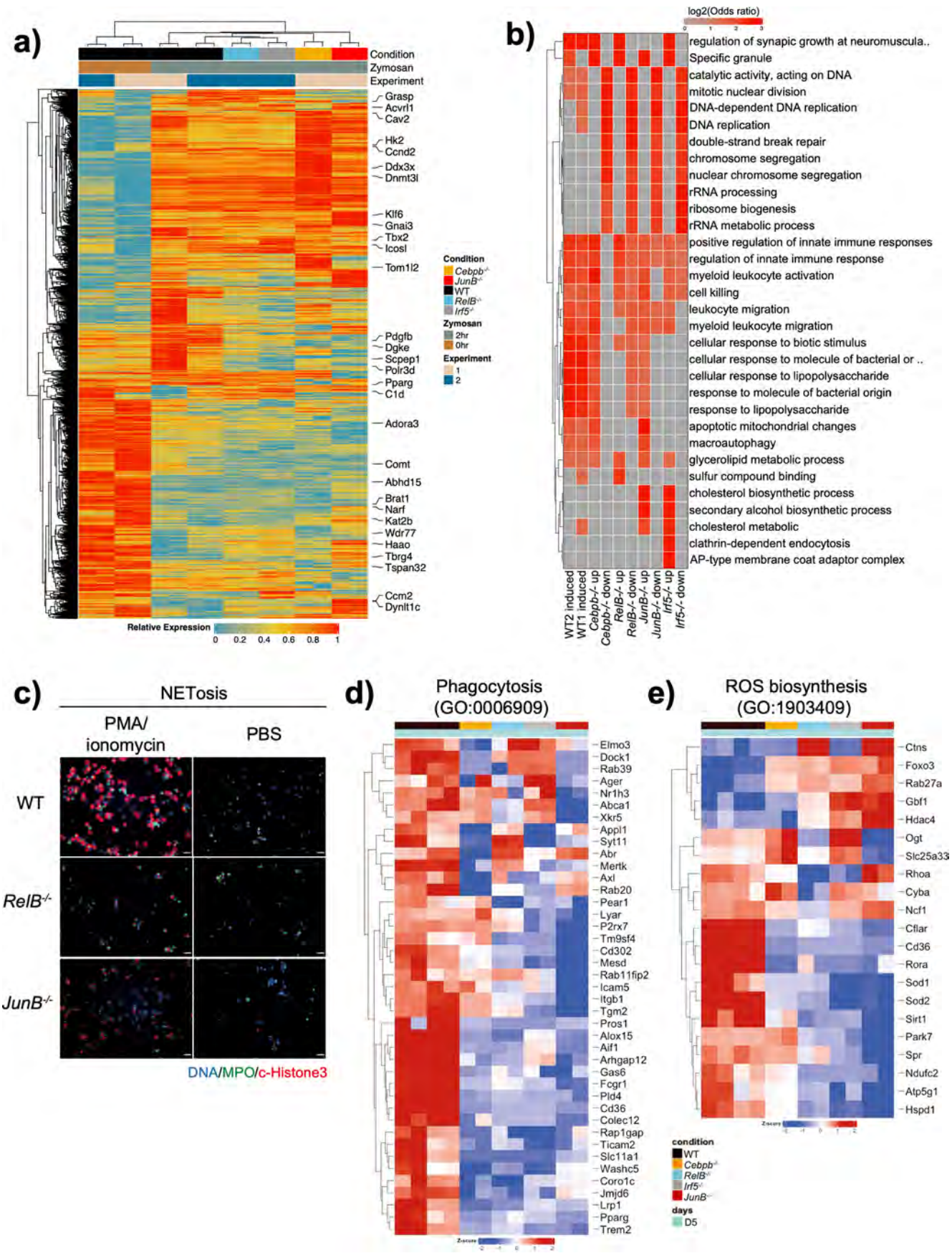

Extended Data Fig. 8 | See next page for caption.

Extended Data Fig. 8 | RELB, IRF5, and JUNB deficiency impair neutrophil inflammatory responses. a, Hierarchical clustering of all DEGs (padj < 0.05, |log2FC|>1). Data are presented as heatmap normalized to the minimum and maximum of each row. **b**, Gene ontology (GO) analysis showing the log2 odds ratio of genes regulated by specific TF knockout with the indicated GO annotation. **c**, Representative immunofluorescence images of NETosis from WT, *RelB*$^{-/-}$ and *JunB*$^{-/-}$ HoxB8 neutrophils stimulated with 5 μM ionomycin and PMA overnight, stained for DNA (blue), MPO (green) and citrullinated histone3 (red). Representative images from three independent experiments are shown. Scale bar indicates 10 μm. **d**, Phagocytosis-related gene expression in in *Cebpβ*$^{-/-}$, *RelB*$^{-/-}$, *Irf5*$^{-/-}$ or *JunB*$^{-/-}$ HoxB neutrophils. **e**, ROS-biosynthetic-process-related gene expression in WT, *Cebpβ*$^{-/-}$, *RelB*$^{-/-}$, *Irf5*$^{-/-}$ or *JunB*$^{-/-}$ HoxB8 neutrophils.

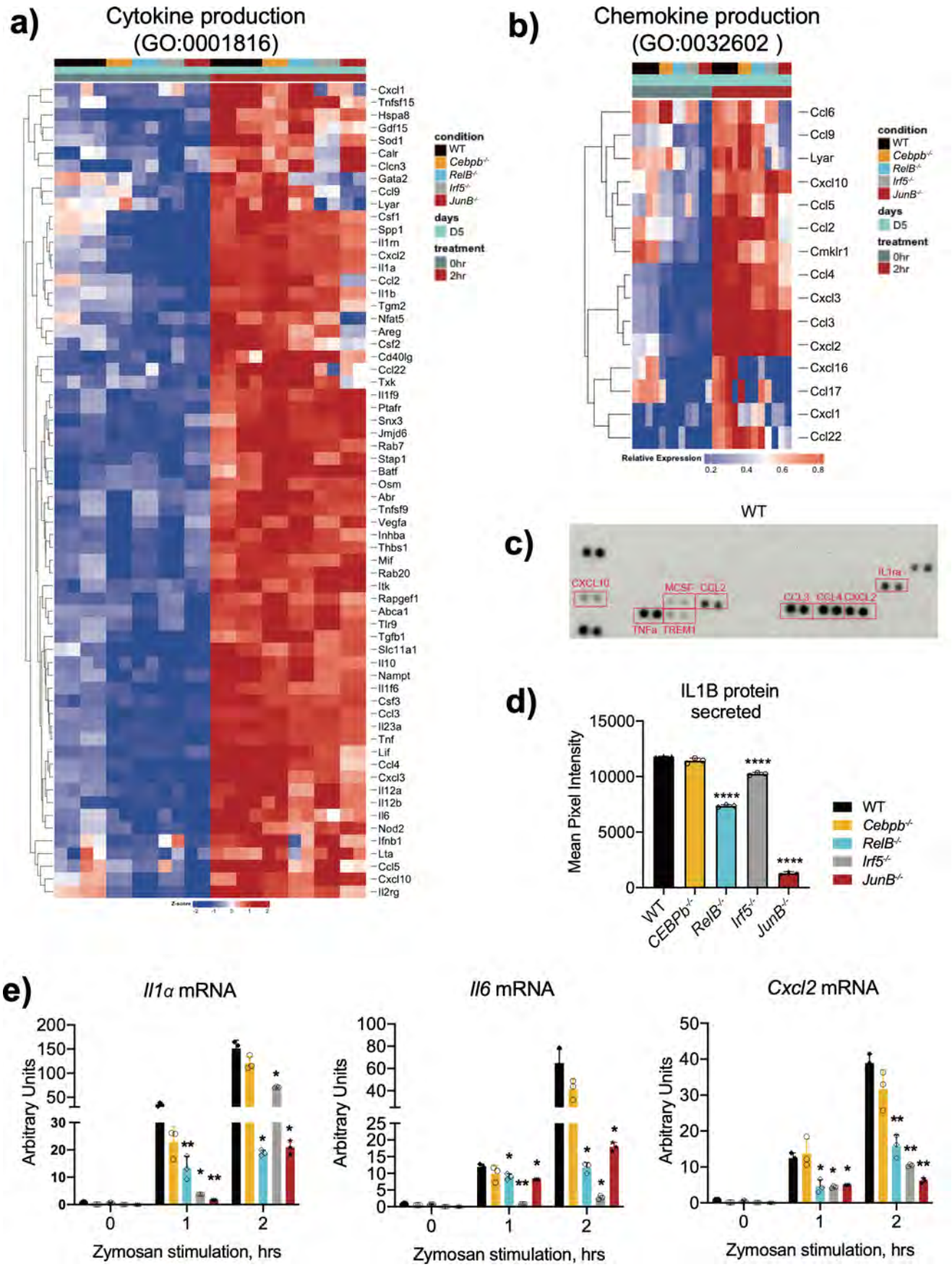

Extended Data Fig. 9 | See next page for caption.

Extended Data Fig. 9 | RELB, IRF5, and JUNB affect neutrophil inflammatory gene expression and production. a, Cytokine-production-related gene expression in WT, *Cebpβ*$^{-/-}$, *RelB*$^{-/-}$, *Irf5*$^{-/-}$ or *JunB*$^{-/-}$ HoxB8 neutrophils. **b**, Chemokine-production-related gene expression in *Cebpβ*$^{-/-}$, *RelB*$^{-/-}$, *Irf5*$^{-/-}$ or *JunB*$^{-/-}$ HoxB8 neutrophils. **c**, *Il1α, Il6* and *Cxcl2* mRNA induction in HoxB8 neutrophils stimulated with zymosan (50ug/ml) for 0, 1, 2 hours. Gene expression was measured by qPCR. Data are shown as means and SD from three independent experiments. Significant differences compared between KO and WT neutrophils are denoted as: *P < 0.05, **P < 0.01, ****P < 0.0001, and ****P < 0.0001; (DM one-way ANOVA with Dunnett's multiple comparisons test). **d**, Cytokines and chemokines secreted from WT HoxB8 neutrophils challenged with Zymosan for 2 h, measured by the proteome array shown in Fig. 6b. **e**, Densitometric quantification of IL1β secretion from HoxB8 neutrophils stimulated with stimulated with zymosan (50ug/ml) for 2 hours, measured with 30 minutes exposure time. Data are shown as mean and SD of three biologically independent samples. Significant differences compared between KO and WT neutrophils are denoted as: *P < 0.05, **P < 0.01; (Ordinary one-way ANOVA with Dunnett's multiple comparisons test).

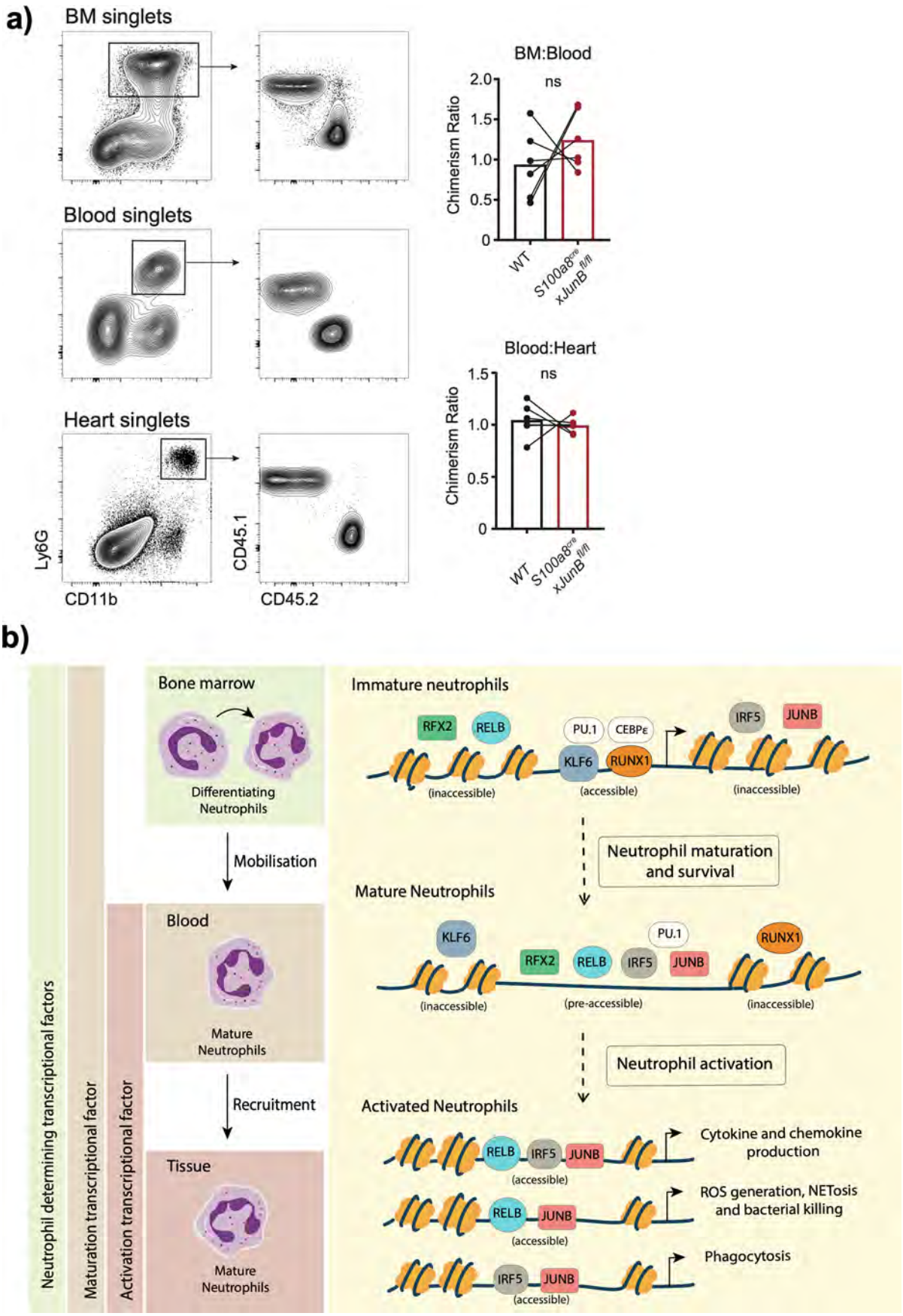

Extended Data Fig. 10 | See next page for caption.

Extended Data Fig. 10 | Assessment of chimerism in MBMC and proposed TF blueprint. a, Representative flow cytometry (left) and the chimerism ratio (right) of neutrophils in the bone marrow, blood, and heart in mice subjected to permanent myocardial infarction 6 weeks after bone marrow transplant. Data are shown as means and SD derived from three mice from each group within one experiment. Statistical comparison was made by paired student-t test. ns, no significant difference. **b**, Model of transcriptional regulation of neutrophils during inflammation. In the process of differentiation in bone marrow, lineage-determining transcriptional factors, including RUNX1, KLF6, CEBPE, and PU.1, are highly expressed and ensure gene expression programmes that promote proper neutrophil maturation. During the mobilization from the bone marrow into the blood, RFX2, RELB, IRF5 and JUNB become upregulated and transcriptionally accessible to support neutrophil cell survival and establish their effector function repertoire, whereas RUNX1 and KLF6 expression are silenced. Upon inflammation, circulating neutrophils migrate into the inflammatory sites, where they are exposed to inflammation-derived signals and become activated. Neutrophil activation leads to the activation of TFs, including RELB, IRF5 and JUNB, and subsequent TF binding to already accessible binding sites, thereby resulting in diverse TFs genomic occupancy and distinct transcriptional outputs.